MAREES TERRESTRES

BULLETIN D'INFORMATIONS

INTERNATIONAL CENTER FOR EARTH TIDES
CENTRE INTERNATIONAL DES MAREES TERRESTRES

International Association of Geodesy - International Gravity Field Service
(IAG – IGFS)

Publié par l'Université de la Polynésie française

BIM n°147

ISSN n° 0542-6766

15 DECEMBRE 2011

Éditeur : Pr. Jean-Pierre BARRIOT
Observatoire Géodésique de Tahiti
Université de la Polynésie française
BP6570 – 98702 Faa'a
Tahiti-Polynésie française

BLANK PAGE

The precious help of Prof. Bernard Ducarme is gracefully acknowledged for his guidance and help in completing this issue of the BIM.

BLANK PAGE

BIM 147

15 décembre 2011

ADMINISTRATIVE MATTERS

BLANK PAGE

Comparison between the Transfer Functions of three Superconducting Gravimeters

O. Francis[1], C. Lampitelli[1], G. Klein[1], M. Van Camp[2] and V Pálinkáš[3]

[1] *University of Luxembourg, Faculty of Sciences, Technology and Communication, Luxembourg*
[2] *Royal Observatory of Belgium, Brussels, Belgium*
[3] *Research Institute of Geodesy, Topography and Cartography, Geodetic Observatory Pecný, Ondřejov, Czech Republic*

Abstract

The transfer functions of the superconducting gravimeters OSG-CT40, SG-C021 and OSG-050 operating in Walferdange (Luxembourg), Membach (Belgium), and Pecný (Czech Republic), respectively, have been experimentally determined by injecting known voltages into the feedback loop of the control electronics. The transfer function is expressed in terms of either its Laplace transforms or by zeros and poles. The latter is widely used in seismology. In particular in the high frequency seismic band, the full transfer function of the Superconducting Gravimeter (SG) is required for data analysis. The results for these three SGs are different enough that the transfer function cannot be calculated theoretically or assumed to be the same for all the SGs. An accurate and precise determination has to be performed for each SG.

1. Introduction

In geophysics, Superconducting Gravimeters (SGs) are used to continuously monitor relative gravity changes. They are the most precise instruments to study of solid earth tides: for instance, it is possible to measure tidal amplitudes in the diurnal and semi-diurnal bands with a precision of about 0.1-0.2 nm/s^2 for integration periods of 2-3 years. Their instrumental drift is extremely low (typically around 10 nm/s^2 per year) and smooth [*Van Camp and Francis, 2007*]. SGs observations are used to monitor the ocean loading effects, to validate the global ocean tides models, to record gravity changes due to the atmosphere, as air mass redistribution and pressure changes related to meteorological events [*Goodkind, 1999*], and to monitor the water storage changes [*Goodkind, 1999, Creutzfeld et al., 2010*]. At higher frequencies, SGs record normal modes of the Earth excited after big Earthquakes [*van Camp, 1999]*.

Some of these applications require a precise determination of the instrumental drift of the SGs. Simultaneous measurements of the SGs side-by-side with an absolute gravimeter has been proved to be very efficient not only to estimate SGs long term drift but also to calibrate the relative SGs. In addition, bad AG values due to malfunctioning of the absolute gravimeter can be detected from regular comparisons with the continuous SG time series.

The knowledge of the transfer function of SGs is essential to fully exploit their observations [*Van Camp, 1998; Van camp et al., 2000*]. Besides analysis of their observations, the transfer functions play an important role when comparing or combining data sets from multiple SGs or other instrumentations as absolute gravimeters or seismometers. To reach optimal performance of SGs in tidal research, where SGs can be considered as world most sensitive instruments, those instruments should be calibrated with an accuracy of 0.1% in amplitude and 0.01 second in phase [*Hinderer et al., 1991, Baker and Bos, 2003*]. Van Camp et al. [2000] were the first to determine experimentally the transfer function of a SG. Step and sine waves voltages are injected into the feedback circuit of the control electronics of the gravimeter and the system response is recorded.

This method was applied to determine transfer function of the cryogenic gravimeter SG-C021 operating in Membach (Belgium), in a series of experiences (1996-2005) for different outputs (depending on the analog filter) and different data acquisition systems. A precision better

than 0.01 second in the phase response (time lag) was obtained. In 2007, the same method was applied to determine the transfer function of the OSG-CT40 operating in Walferdange (Luxembourg), as well as of the OSG-050 operating in Pecný (Czech Republic) (OSG meaning Observatory Superconducting Gravimeter).

In this paper, the calibration experiment carried out in Walferdange is described. The transfer functions obtained for the three gravimeters are then compared. They are represented in terms of Laplace transforms [*Scherbaum, 2001*]. In seismology, this is the standard formulation used by the seismic Incorporated Research Institutions in Seismology (IRIS)) data base [*http:// www.iris.edu*], where some SGs data are archived. In such a Data Base, the information on the transfer function (being considered as important as the observations themselves) is mandatory.

2. Functioning principle of the superconducting gravimeter

In superconducting gravimeters, a hollow superconducting niobium sphere is in equilibrium under the combined action of the gravity force on the sphere and a vertical upward directed levitation force. This force is provided by the magnetic field generated by a pair of superconducting niobium coils with persistent current [*Goodkind, 1999*]. Two coils - their configuration respect to the sphere and the ratios of currents in the coils - allow one to independently adjusting the total levitating force and the force gradient in such a way that a small change in gravity can induce a large variation in the sphere vertical position. This variation is detected by an electrostatic device (a capacitance bridge constituted by three capacitor plates and the levitating sphere) and a feedback magnetic force (generated by a feedback coil) brings the sphere back to its initial position. The feedback integrator voltage is linearly proportional to changes in the acceleration of gravity. To allow the stable levitation to occur, the gravity sensor (Figure 1) must be maintained in a condition of superconductivity (niobium is superconducting below 9.3 K). This is realized by placing the gravity sensor inside a Dewar filled with liquid helium (4.2 K boiling point).

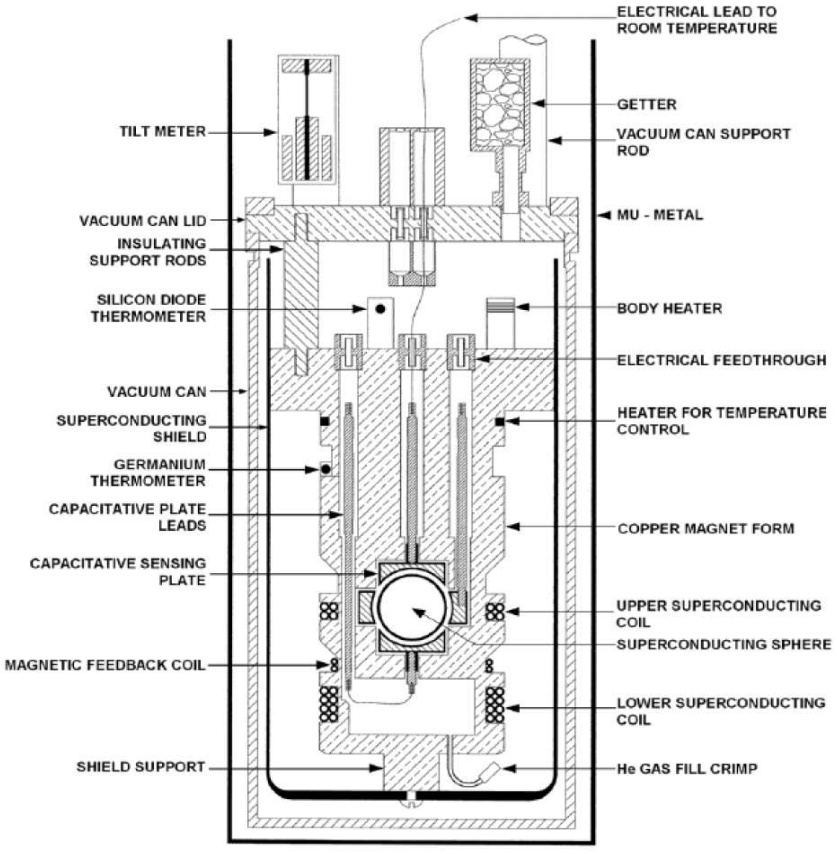

Figure 1. Gravity sensor unit of the Superconducting Gravimeter (Figure from the GWR Manual).

The unique characteristics of SGs lie in the continuity of the gravity signal registration, the linearity and stability of feedback system, the very high sensitivity (5 $(nm/s^2)^2/Hz$ corresponding to a precision of 0.2 nm/s^2 (or 0.02 μGal) at a period of 100 s [*Van camp et al., 2005; Rosat et al, 2009*] and a low instrumental drift of a few μGal/year [*Van Camp and Francis*, 2007].

The instrument calibration can be obtained by fitting the SG observed signal to known signals (i.e. Earth tides or modeled inertial effects). It can be further improved by comparing the SG observations to simultaneous absolute gravity measurements in a nearby location. Francis et al. (1998) showed that accuracy on the amplitude calibration factor of 0.1% can be achieved within 4 days of observations during high tides. However, this method does not provide a reliable phase calibration. This latter requires another type of experiment to determine the transfer function.

The feedback voltage is the output signal from the SG gravity control card (Figure 2, upper part). On the card, an analog low-pass filter is provided as an anti-aliasing filter for digitizing the gravity signal. The card and the filter significantly affect the transfer function of SGs.

For the SG-C021, the feedback voltage was provided with the use of three different cards [*Van Camp et al. 2000, Van Camp et al. 2008*]. Until 1997, the electronics was provided with a 6-pole Butterworth tide filter and a card with a 2-pole Butterworth Gravity Signal (GS) with cutoff periods at 72 second and 1 second, respectively. Since 1997, in order to fulfill the Global Geodynamics Project (GGP) requirements [*Crossley et al., 1999*] and to improve the quality of the electronics with up to date components, a card with an 8-pole Butterworth low-pass filter (GGP-1) and cutoff period at 16 second replaced the old version.

Currently, most of the superconducting gravimeters are equipped with a GGP-1 filter or, alternatively, a GGP-2 filter, having cutoff period at 32 second.

The transfer function determinations for the SG-C021 were also conducted for different data acquisition systems, i.e. K2000 voltmeters and a Quanterra 330 data logger. Van Camp et al. [2008] concluded that both the low-pass filter characteristics and the data acquisition system characteristics have an effect on the instrument response.

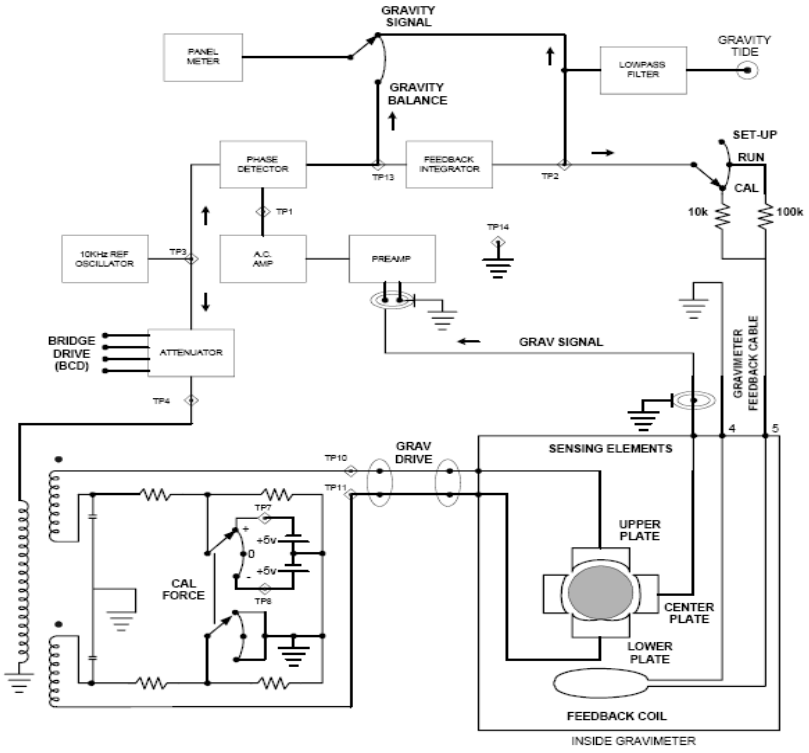

Figure 2. Scheme of the superconducting gravimeter control electronics. The gravity control card includes the feedback integrator and the low-pass filter (Figure from the GWR Manual).

3. The Laplace transform and the transfer function

The Laplace transform represents a powerful differential instrument for the analysis of Linear Time Invariant systems (LTI), such as electronic circuits [*Bertoni et al., 2003, Ambardar, 1995, Beerends et al., 2003*]. The Laplace operator acts on functions in the time domain, transforming them into functions in the frequency domain. The system input and output are functions of the complex angular frequency or Laplace variable, usually denoted *s*, expressed in radians per unit of time.

If *f(t)* represents a real function of time defined for positive values of the time variable *t*, the Laplace Transform of *f(t)* is defined as

$$\mathcal{L}[f(t)] = F(s) = \lim_{\substack{T\to\infty \\ \varepsilon\to 0}} \int_{\varepsilon}^{T} f(t)\cdot e^{-st}dt = \int_{0+}^{\infty} f(t)\cdot e^{-st}dt \qquad 0<\varepsilon<T \tag{1}$$

where *s* is a complex variable defined by $s=\sigma+i\cdot\omega$.

The differential Laplace operator is a linear operator. The Laplace Transform of the time derivative of a function *f(t)* having *F(s)* as Laplace transform, is expressed as

$$\mathcal{L}\frac{df(t)}{dt} = s\cdot F(s) - f(0^{+}) \tag{2}$$

The Laplace Transform of the time integral of a function *f(t)* having *F(s)* as Laplace transform, is expressed as

$$\mathcal{L}\left[\int_{0}^{t} f(\tau)d\tau\right] = \frac{F(s)}{s} \tag{3}$$

Laplace transform provides solutions to the differential equations characterizing LTI systems, reducing them to more easily solvable algebraic relations.

4. Transfer function and frequency response for LTI systems

A transfer function (or network function) for a LTI system is a mathematical relationship (in the spatial or temporal frequency domain) between the model output and input [*Di Stefano et al., 2004*]. In the case of continuous input signal *x(t)* and output signal *y(t) in time domain*, the transfer function of a LTI system can be expressed as the ratio between the output Laplace transform Y(s) and the input Laplace transform X(s):

$$H(s) = \frac{Y(s)}{X(s)} \tag{4}$$

where $X(s)= \mathcal{L}[x(t)]$ and $Y(s)= \mathcal{L}[y(t)]$. The transfer function also corresponds to the Laplace transform of the system's impulse response.

For LTI systems, because of the previously underlined properties of the Laplace transform, the transfer function is generally represented by the ratio of two polynomials of the Laplace complex variable *s*:

$$H(s) = \frac{\sum_{j=0}^{m} b_j s^j}{\sum_{j=0}^{n} a_j s^j} \tag{5}$$

The poles/zeros are defined as the values of s for which the denominator/numerator of the transfer function is equal to zero [*Scherbaum, 2001*]. In the time domain, each pole is associated with a response mode of the system. The impulse response of the system is a linear combination of the different response modes. Thus, the transfer function completely defines the system response.

If the input of a LTI system is a sinusoidal signal with frequency ω (rad/s), it can be represented in complex form:

$$x(t) = |X| \cdot e^{i(\omega t + \varphi_X)} = |X| \cdot e^{i\varphi_X} \cdot e^{i\omega t} = X \cdot e^{i\omega t} \tag{6}$$

where $|X|$ is the input amplitude, φ_X the input phase and i represents the imaginary number. The corresponding system output is also a sinusoidal signal having the same frequency ω but generally a different phase and amplitude:

$$y(t) = |Y| \cdot e^{i(\omega t + \varphi_Y)} = |Y| \cdot e^{i\varphi_Y} \cdot e^{i\omega t} = Y \cdot e^{i\omega t} \tag{7}$$

where $|Y|$ is the output amplitude and φ_Y the output phase. The amplitude frequency response represents the ratio between the output and input amplitudes as a function of the frequency ω, and is defined as the gain:

$$G(\omega) = \frac{|Y(\omega)|}{|X(\omega)|} \tag{8}$$

The phase frequency response represents the difference between the output and input phases as a function of the frequency ω:

$$\phi(\omega) = \varphi_Y(\omega) - \varphi_X(\omega) \tag{9}$$

For a discrete frequencies sample the frequency response in complex form is

$$R(\omega_n) = \frac{|Y_n|}{|X_n|} \cdot e^{i\cdot\phi_n} = G_n \cdot e^{i\cdot\phi_n} = \frac{Y_n}{X_n}\ , \qquad n=1\text{: frequency sample length} \tag{10}$$

where, for an input signal at frequency ω_n, G_n and Φ_n represent the gain and the phase shift, respectively.

Least-squares fit algorithms allow one to determine the polynomial coefficients of the transfer function H_s (Eq. 5) from the experimental frequency response in complex form (Eq. 9), determined on a limited chosen frequencies. Conversely, the frequency response in complex form, and consequently the gain and phase lag, can be derived from the transfer function H_s where the variable s is replaced with the variable $(\omega \cdot i)$ for positive values of ω.

5. Experimental determination of the frequency response for the OSG-CT40

The frequency response for the OSG-CT40 operating in Walferdange (Luxembourg) was determined using the *Van Camp et al.* [2000] procedure. The frequency response was experimentally obtained by injecting step functions and sine waves (input signal) at defined voltages into the feedback loop of the gravimeter. The output signal was taken from the GGP-1 low pass filter.

In the step function method [*Richter and Wenzel, 1991; Wenzel, 1994; Van Camp et al., 2000*], the step response function is differentiated to obtain the impulse response function. The Fourier spectrum of the impulse response function corresponds to the transfer function of the system [*Bloomfeld, 1976, Van Camp et al., 2000*]. In the sine wave method, the transfer function is obtained by fitting both the input signal (waves injected at different frequencies) and the output signal (instrument response) with a sinusoidal function. The amplitude ratios and phase differences as a function of the input frequencies correspond to the instrumental frequency response (Eq.7 and Eq. 9).

The superconducting gravimeter can be considered as a Linear Time Invariant system [*Goodkind, 1999*]. It means that both sine waves and step functions should provide the same transfer function. The comparison of results from the two methods gives the opportunity to assess their accuracy.

29 time steps and sine waves, with 4 Volt amplitude, at four different periods (200 second, 500 second, 1000 second and 2000 second) were injected into the feedback loop of the control electronics of the SG. The instrument frequency responses obtained with the sine wave and the step function methods are given in Table 1 and displayed in Figures 3. As expected and found previously by Van Camp et al. (2000), both methods give similar results consistent within their uncertainties.

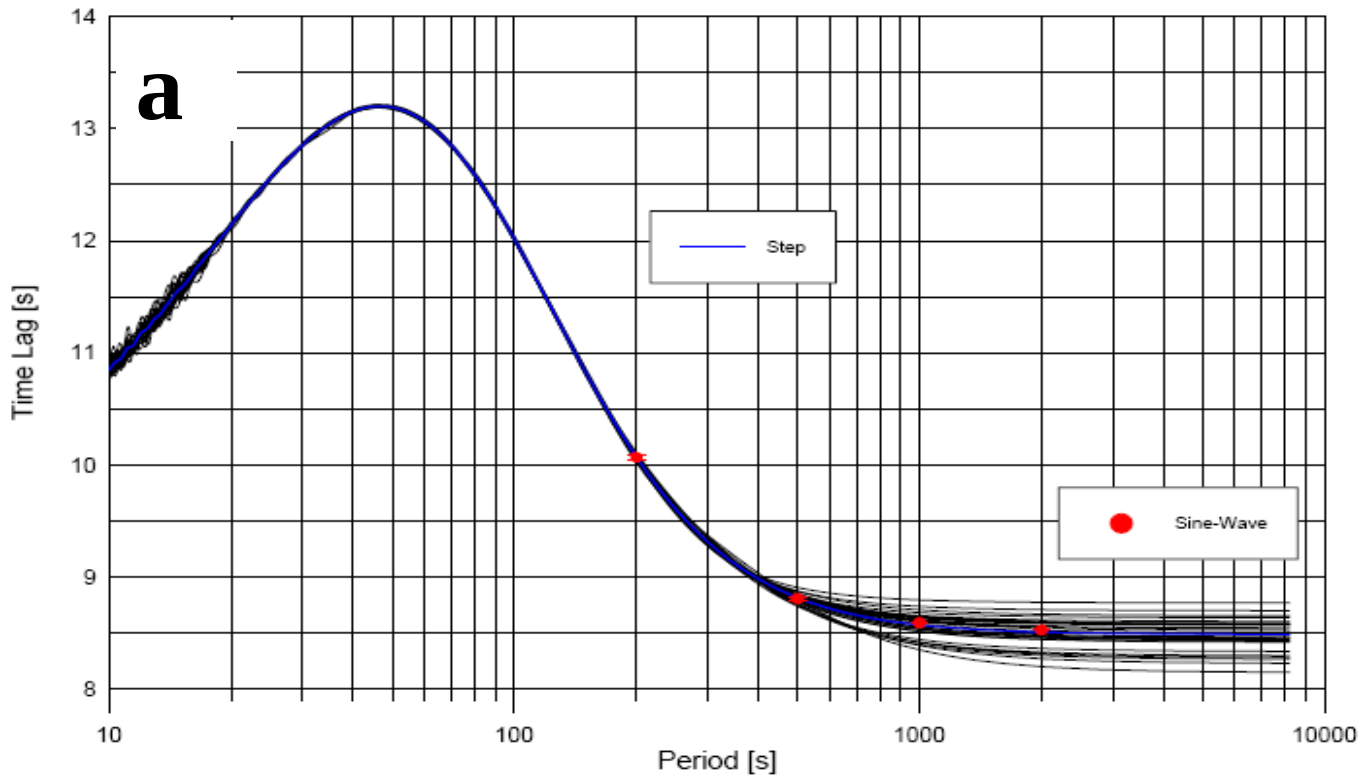

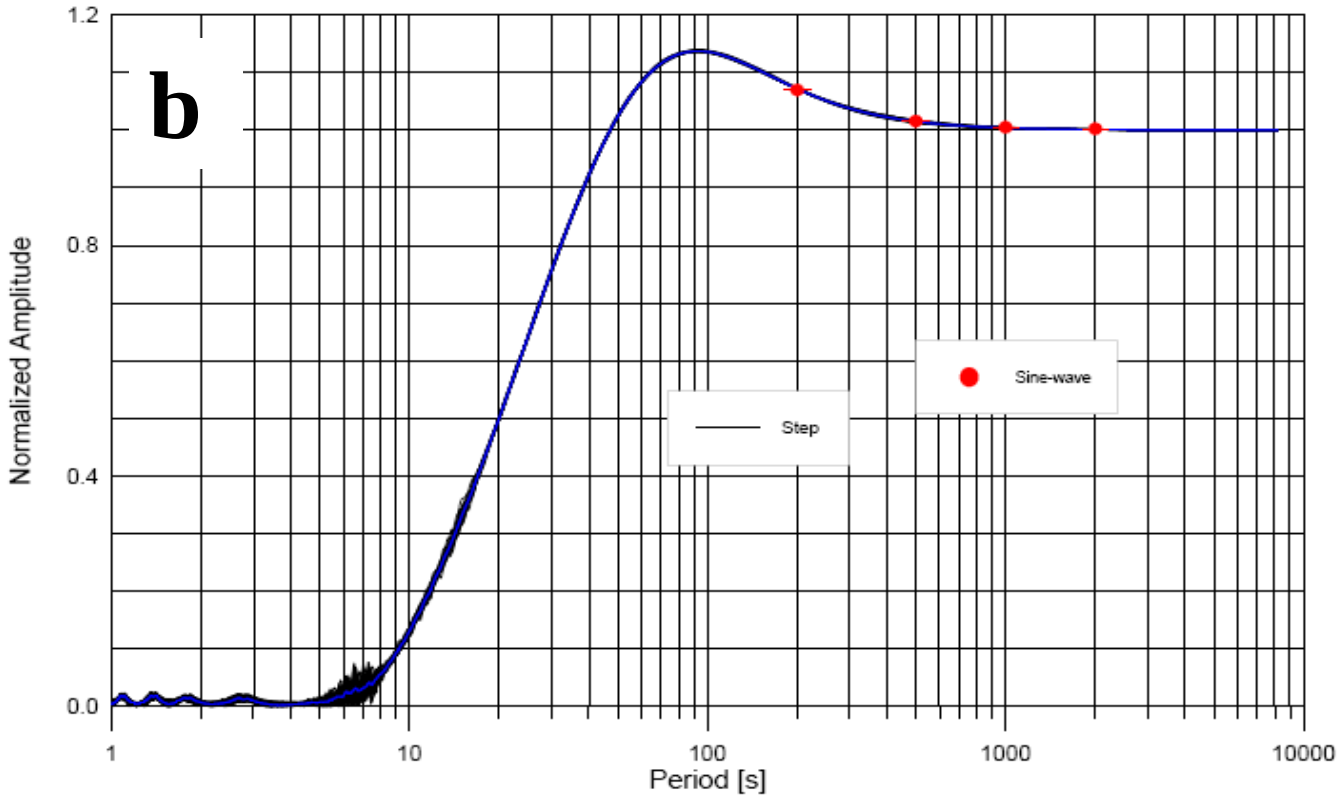

Figures 3. Frequency response of the OSG-CT40 obtained by injecting sine waves (red dots) and step functions (continuous line) into the instrument electronics: a. Phase as a function of period represented in terms of time lag (s); b. Normalized amplitudes a function of period.

Table 1. Time lags and normalized amplitudes of the OSG-CT40 obtained, for four different periods, using the sine waves and the step functions methods.

Period/ second	Sine Waves Time lag/second	Step functions Time lag/second	Sine Waves Amplitude	Step functions Amplitude
200	9.818+-0.011	9.823+-0.017	1.044374+-0.000353	1.0469+-0.0004
500	8.571+-0.011	8.554+-0.042	0.990787+-0.000138	0.9892+-0.0130
1000	8.343+-0.003	8.323+-0.111	0.980199+-0.000022	0.9787+-0.0005
2000	8.281+-0.020	8.256+-0.136	0.977218+-0.000006	0.9759+-0.0001

6. Comparison between the transfer functions of the three gravimeters

In this section, we compare the frequency responses of the OSG-CT40 in Walferdange (experiment of 2007) with the ones of the SG-C021 in Membach (experiment of 2005) and of the OSG-050 in Pecný (experiment of 2007). The transfer function of the OSG-050 was determined using only step functions with voltages of 10 Volt and 15 Volt.

In the three experiments, the GGP-1 filter output was used. For the SG-C021, the output data were acquired with a Quanterra 330 data logger [*Van Camp et al., 2008*]. The amplitude and phase responses of the three instruments are displayed in Figures 4.

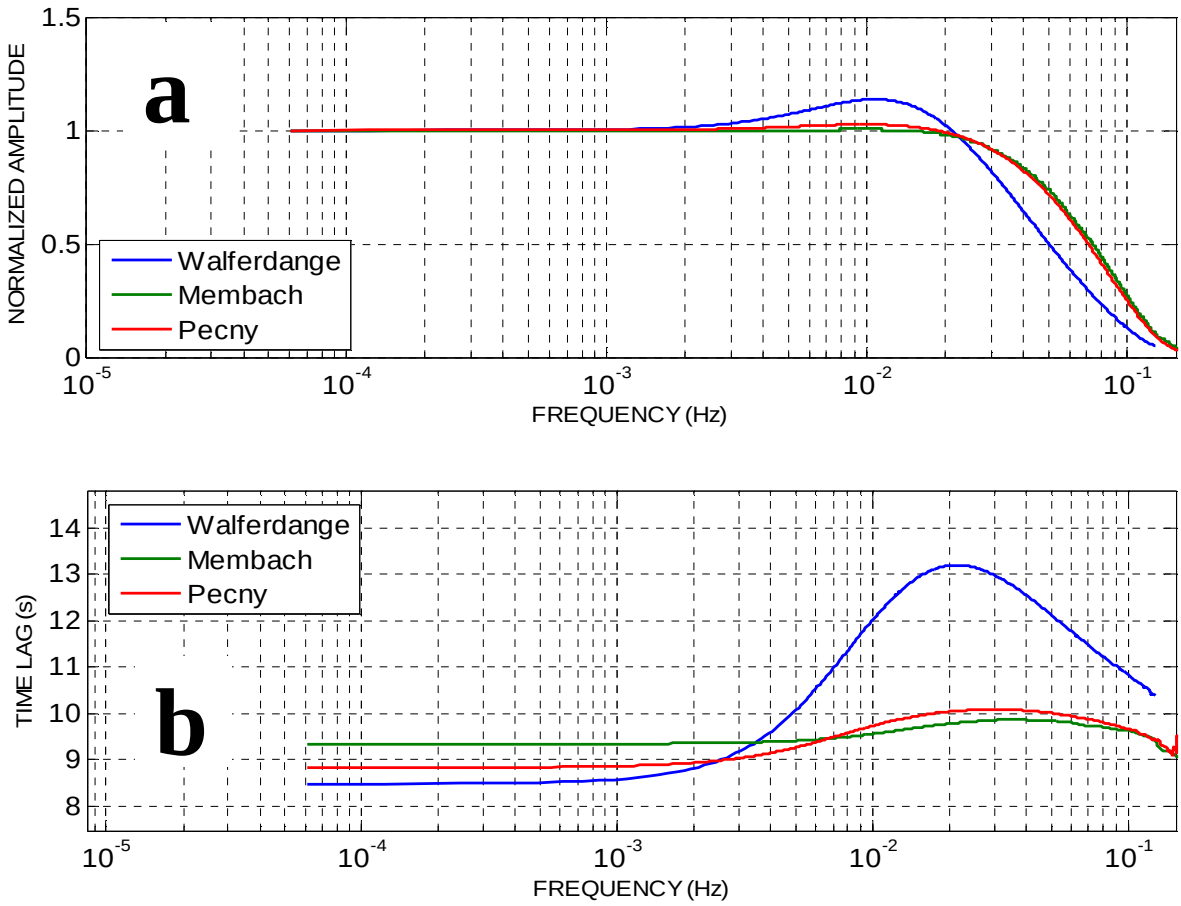

Figures 4. Normalized amplitude responses (a) and time lag (b) experimentally determined for the OSG-CT40 (blue), the SG-C021with the Quanterra 330 data logger (green) and the OSG-050(red).

The frequency responses, especially in phase, are significantly different in shape, for frequencies higher than 10^{-3} Hz. Differences up to 30% for the phase and up to 10% for the amplitude are observed.

The polynomial coefficients of the transfer functions are obtained from the complex experimental frequency response with a least-squares fit. The form of the transfer function is defined by the ratio of two polynomials of the complex Laplace variable *s* (Eq. 5). For the three gravimeters, the numerator and denominator of the transfer function are best modeled as 6^{th} order polynomials of the Laplace variable *s*. Lowest orders are not sufficient to match the experimental transfer functions while highest orders do not improve the fit. For the OSG-CT40, the average difference between the modeled and observed values of the frequency response is $3 \cdot 10^{-5}$ in amplitude and $6 \cdot 10^{-5}$ second in phase. Similar results are obtained for the other gravimeters.

We stress that the order of the denominator must be equal or superior to the order of the numerator, otherwise the gain would be unbounded for increasing frequencies.

From the transfer function *H(s)*, the instrument frequency response (amplitude and phase) is calculated by replacing in equations (11), (12) and (13) the variable *s* with the variable $(\omega \cdot i)$. The transfer functions for the three SGs are:

- OSG-CT040

$$H(s) = \frac{-0.03897s^6 + 0.08883s^5 - 0.1268s^4 + 0.1159s^3 - 0.06664s^2 + 0.01835s + 0.0010281}{s^6 + 1.744s^5 + 1.6s^4 + 0.8269s^3 + 0.2292s^2 - 0.0271s + 0.001028} \quad (11)$$

- SG-C021

$$H(s) = \frac{0.02815s^6 + 0.02244s^5 - 0.01175s^4 + 0.02098s^3 - 0.02972s^2 + 0.01456s + 0.002007}{s^6 + 1.324s^5 + 1.215s^4 + 0.628s^3 + 0.202s^2 - 0.03342s + 0.002007}$$

(12)

- OSG-050

$$H(s)=\frac{-0.07454s^6+0.1751s^5-0.2599s^4+0.2502s^3-0.1558s^2+0.04905s+0.002634}{s^6+2.043s^5+2.149s^4+1.305s^3+0.4478s^2-0.07236s+0.002634} \quad (13)$$

In Figures 5, the poles and zeros of the transfer functions for the three gravimeters are shown. The poles are the values of *s* that make the denominator of the transfer function equal to zero leading to the divergence (i.e. instability) of the transfer function. As previously pointed out, each pole is associated, in the time domain, to a mode of the instrument response, which is expressed by:

$$y_h(t)=\sum_{i=1}^{n} C_i \cdot e^{p_i \cdot t} \quad (12)$$

where *p* represents the poles in complex form and *C* are constants depending on the initial conditions.

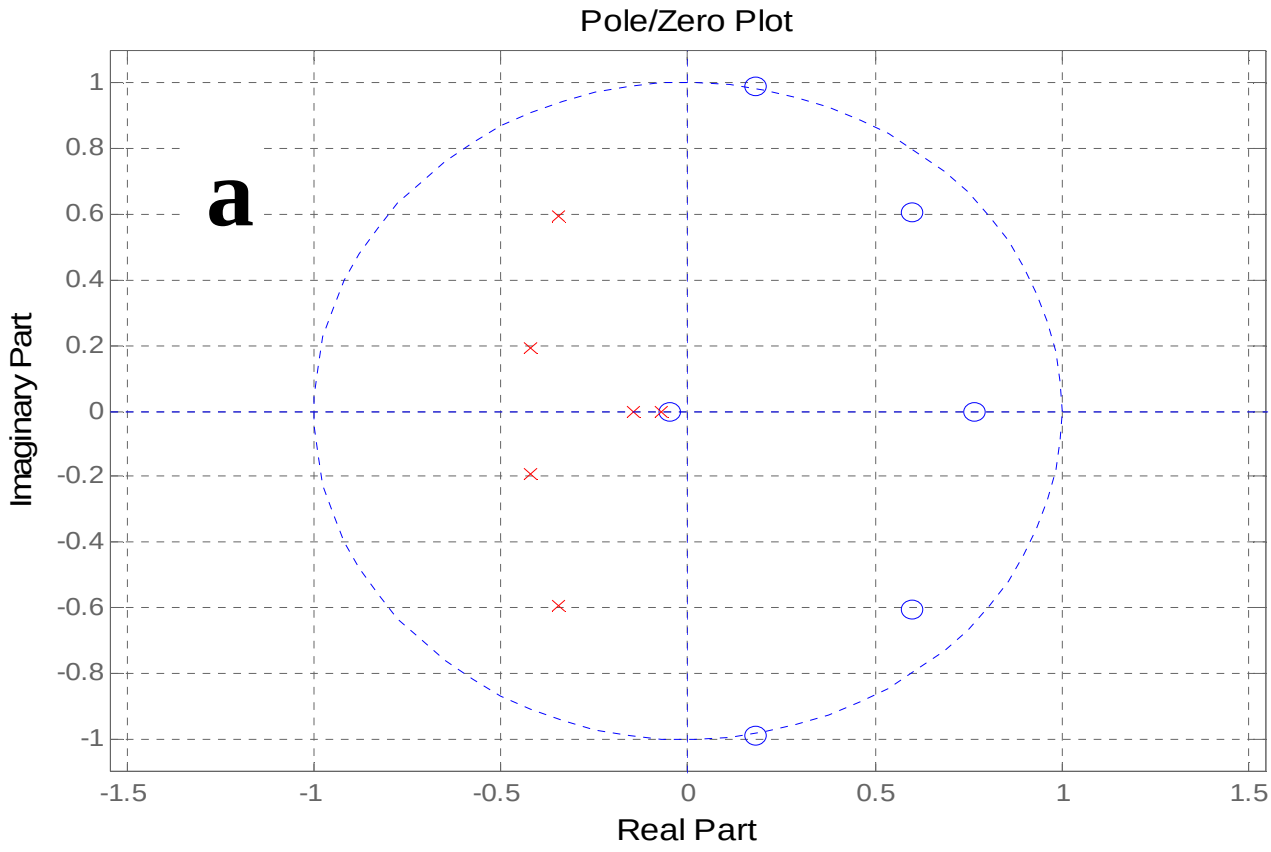

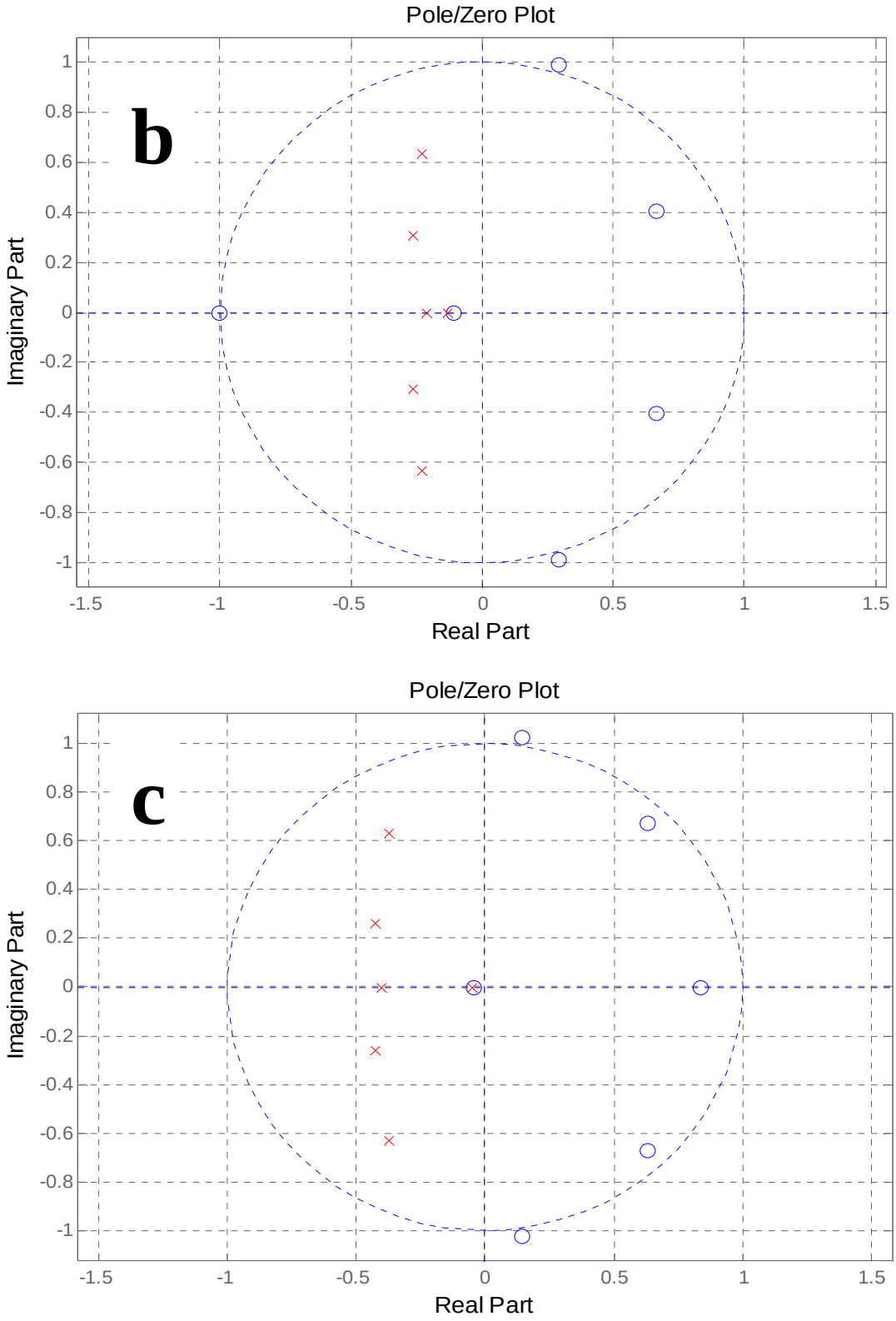

Figures 5. Pole-Zero plots: representation in the complex coordinate system of the points corresponding to the poles and zeros of the transfer function, for the OSG-CT040 (a), the SG-C021 (b) and the OSG-050 (c). The poles are represented with red crosses; the zeros are represented with blue circles.

From the pole-zero diagrams (Figures 5), some qualitative observations on the systems responses can be drawn. For the three instruments, the poles are all located in the left half of the *s* plan (real part <0). This implies that all the response components tend to 0 for *t* tending to infinite, and consequently the systems stability.

The response is qualitatively similar for the three gravimeters. The three systems are characterized by two pairs of conjugate complex poles, corresponding to two sinusoidal decaying response components, and two real poles, corresponding to two exponentially decaying response components. The differences lie in the decay rates (defined by the poles real part) and the frequency of the oscillations of the sinusoidal modes (defined by the poles imaginary part). The nearest the pole is to the imaginary axis, the slowest is the decay rate. The nearest the pole is to the real axis, the lowest is the oscillation frequency. The response component with the slowest decay rate represents the dominant response mode.

For the three gravimeters, the dominant modes are exponential terms with different decay rates. The dominant terms for the OSG-CT040, the SG-C021 and OSG-050 persist approximately for 56 s, 30 s and 80 s, respectively.

Conclusions

The frequency response (amplitude and time lag) of the OSG-CT40 from Walferdange in Luxembourg has been experimentally determined using the procedure of Van Camp et al. (2000). The same precision and accuracy as this previous study were obtained.

The transfer functions from three SGs were also compared. The differences can reach 10% in amplitude and 30% in phase in the seismic band at frequencies higher than 10^{-3} Hz.

For a complete and accurate calibration of SGs, we recommend to the SG operators to carry out the same procedure. The transfer function is definitively unique for each superconducting gravimeter (including the gravity control card and the data acquisition system). We also encourage expressing the transfer function in terms of Laplace Transforms, which is widely used in seismology. It provides a compact and efficient way to express the transfer function. Its determination is essential to analyze and interpret the SGs' observations especially in the seismic frequency band.

References

Ambardar, A. (1995). Analog and digital signal processing, 330 pp., Brooks/Cole Publishing Company.

Baker, T.F., Bos, M.S.(2003). Validating Earth and ocean tide models using tidal gravity measurements. Geophys. J. Int. 152, 468–485.

Beerends, R. J., ter Morsche H. G., van der Berg, J. C., van de Vrie, E. M. (2003). Fourier and Laplace Transforms . 458 pp., Cambridge University Press.

Bertoni A., Campadelli P., Grossi G. (2003). Introduzione alla elaborazione dei segnali, 102 pp., Università degli studi di Milano.

Bloomfield, P.(1976). Fourier analysis of time series: an introduction, John Wiley & Sons, New York, 1976.

Creutzfeldt, B., Güntner, A., Vorogushyn, S., and Merz, B. (2010). The benefits of gravimeter observations for modelling water storage changes at the field scale, Hydrol. Earth Syst. Sci. Discuss., 7, 2221-2260, doi:10.5194/hessd-7-2221.

Crossley, D., Hinderer, J., Casula, G., Francis, O., Tsu, H.-T., Imanishi, Y., Jentzch, G., Kääriänen, J., Meurers, B., Neumeyer, J., Pagiatakis, S., Richter, B., Shibuya, K., Sato, T., and van Dam, T. (1999). The Global Geodynamics Project, EOS Trans. AGU, 80(11), 121, 125-126.

Di Stefano, J. J., Stubberud, A. R., Williams, I, J. (1994). Systèmes asservis, 506 pp., Mc Graw-Hill (UK), Ltd.International

Francis, O. (1997). Calibration of the C021 superconducting gravimeter in Membach (Belgium) using 47 days of absolute gravity measurements. Int. Ass. Of Geodesy Symp., 117-212-218, Springer Verlag.

Francis O., Niebauer T.M., Sasagawa G., Klopping F.J. and Gschwind J.J., (1998). Calibration of a superconducting gravimeter by comparison with an absolute gravimeter FG5 in Boulder, Geophysical Research Letters, VOL. 25, NO.7, 1075-1078, 1998.

Goodkind, J. M. (1999). The superconducting gravimeter. Review of scientific instruments, Volume 70, Number 11, 4131-4152.

Hinderer, J., Florsch, N., Makinen, J.,Legros, H., and Faller, J. E. (1991). On the Calibration of a Superconducting Gravimeter using Absolute Gravity Measurements. Geophysical Journal International, 106, 491-497.

Rosat, S., Boy, J.-P., Ferhat, G., Hinderer, J., Amalvict, M., Gegout, P. & B. Luck, (2009). Analysis of a ten-year (1997-2007) record of time-varying gravity in Strasbourg using absolute and superconducting gravimeters: new results on the calibration and comparison with GPS height changes and hydrology, J. of Geodyn., 48, 360-365.

Scherbaum, F. (2001).Of Poles and Zeros. Fundamentals of Digital Seismology, 2nd Edition, 274 pp., Kluwer Academic Publishers.

Richter, B. and Wenzel, H.-G. (1991). Precise instrumental phase lag determination by step response method, Bull. Inf. Marées Terrestres, 111, 8032-8052.

Van Camp M. (1998). Qualification d'un gravimètre cryogénique pour les périodes supérieures à 100 secondes, PhD thesis, Catholic University of Louvain, Louvain-la-Neuve, 208 pp.

Van Camp, M. (1999), Measuring seismic normal modes with the GWR C021 superconducting gravimeter, Phys. Earth Planet. Inter., 116, 81-92.

Van Camp M., Francis O.(2006). Is the instrumental drift of superconducting gravimeters a linear or exponential function of time?, J. Geod. 81:337-334.

Van Camp, M., Wenzel, H.-G., Schott, P., Vauterin, P., and Francis, O. (2000). Accurate transfer function determination for superconducting gravimeters. Geophysical Research Letters 27 (1), 37-40.

Van Camp M. and O. Francis, (2007) Is the instrumental drift of superconducting gravimeters a linear or exponential function of time?, Journal of Geodesy, 81, DOI10.1007/s00190-006-0110-4, 337-344.

Van Camp, M., Williams, S.D.P., Francis, O. (2005). Uncertainty of absolute gravity measurements . Journal of Geophysical Research 110, B05406.

Van Camp, M., Steim, J.,Rapagnani, G., Rivera, L. (2008). Connecting a Quanterra data logger Q330 to the GWR-C021 Superconducting Gravimeter. Seismological Research Letters, Vol. 79, n.6, 785-796.

Wenzel, H.-G. (1994). Accurate instrumental phase lag determination for feedback gravimeters. Bulletin d'information des Marees Terrestres, 118, 8, 735-752.

Investigations to improve the Signal-to-Noise-Ratio in Data from Superconducting Gravimeters in the Short-Period Spectral Range

J. Wünsch[1], C. Kroner[2], Chr. Förste[3], B. Fersch[4].

1- *Helmholtz Centre Potsdam GFZ German Research Centre for Geosciences, c/o DLR Oberpfaffenhofen, D-82230 Wessling, Germany*
2- *Formerly: Helmholtz Centre Potsdam GFZ German Research Centre for Geosciences, now: Physikalisch-Technische Bundesanstalt, Bundesallee 100, D-38114 Braunschweig, Helmholtz Centre Potsdam GFZ German Research Centre for Geosciences, c/o DLR Germany*
3- *Helmholtz Centre Potsdam GFZ German Research Centre for Geosciences, Telegrafenberg, D-14473 Potsdam, Germany*
4- *KIT, IMK-IFU, Kreuzeckbahnstrasse 19, D-82467 Garmisch-Partenkirchen, Germany*

Corresponding author: J. Wünsch, e-mail: wuen (at) gfz-potsdam.de

Abstract:
The noise level in processed time series from superconducting gravimeters (SG) is mainly caused by not fully reduced atmospheric and hydrological influences. Therefore, we investigated whether an improvement compared to usual reduction methods can be achieved by using: i) highly resolved (both temporally and spatially) 2D surface data of air pressure and temperature in an approach according to Merriam (1992); ii) 3D atmospheric model data (from the WRF) with explicit consideration of the humidity of the air and its distribution.
However, our studies showed that both the 2D- as well as the 3D-atmospheric correction do not give an improvement in the noise level of SG gravity residuals at periods between 2 h and 48 h. This means that the available meteorological 2D- and 3D-datasets are not yet sufficient for an improved reduction of atmospheric influences in the short period spectral range and that the standard air pressure reduction method (using a regression coefficient, i.e. an admittance) is still the most effective reduction method in the short-period spectral range.

1. Goals of our research:

Data from superconducting gravimeters (SG) are nowadays an essential tool to explore global geodynamic phenomena, such as mass displacements or deformations of the crust. SG show a high long-time stability and generally a better signal-to-noise ratio (SNR) than spring instruments (Rosat and Hinderer 2011).

In the search for smallest geodynamic signals it is a prerequisite to eliminate further disturbances from SG time series which manifest themselves as different kinds of noise. During the last years, clear improvements were obtained in the long-period spectral range due to air pressure reduction using 3D atmospheric model output (e.g., Abe et al. 2010, Klügel and

Wziontek 2009). In the short-period spectral range, such a progress in improvements of SNR has not yet occurred. Especially for periods between 2 h and 2 d, an increase of the SNR would be very desirable, as a number of important geodynamic signals is theoretically expected to exist, as for example:

- Translational oscillations of the solid inner core of the Earth, the so-called Slichter mode with a period larger than 5 h (split into a triplett due to Earth rotation and ellipticity).
- Rotational oscillations in the outer, fluid core with anticipated periods of about 24 h and 17 h.

Furthermore, an increase in the SNR in the period range up to 48 h would allow an improved determination of station-specific Earth tide parameters and hence a better data basis for evaluating ocean tide models and loading Love numbers. Despite of existing reduction methods, atmospheric effects still are the greatest disturbing influence in this period range.

The goal of this study was to clarify whether an improvement of reduction of atmospheric influences in observed terrestrial gravity time series can be obtained, if we use:

- Observed highly resolved (spatially and temporally) surface data (pressure p, temperature T), and:

- Modeled 3D-atmospheric-data including the humidity of the air (i.e., without the use of a virtual temperature).

2. Data used and methods of reduction

The two types of data sets (2D and 3D) as used in the present study mainly cover the area of Germany, as there are three existing SG stations and a meteorological observation network is available for Germany. But we focused on the stations Moxa (MO) and Bad Homburg (BH) only. The third mentioned station Wettzell (WE) which is close to the border of the Czech Republic was not involved because of two reasons:

i) The air pressure and temperature data from the Czech Meteorological Service were too expensive and were not available in the favored spatial resolution;

ii) Wettzell displays significant, very locally caused hydrological effects, whose adequate reduction is not yet possible (e.g., Klügel and Wziontek 2009, Creutzfeldt et al. 2010).

We chose for our study the time interval from January 1 to June 30 in 2006, because in this time interval both the highly resolved surface data and modeled 3D data were available.

As a preparation, the gravity time series of both stations (MO, BH) were filtered to 10 min (for 2D) or 1 h (for 3D) time steps. Small data gaps of up to 2 h were interpolated linearly. Both time series were reduced concerning Earth tides and ocean loading. Tidal as well as non-tidal ocean loading was considered, the latter according to the ocean model OMCT (Dobslaw and Thomas 2007). The gravity time series of the station Moxa was additionally reduced for local hydrological effects (Naujoks et al., 2010).

Then we computed the atmospheric corrections according to the following details:

3. Use of highly resolved surface data (2D), Merriam method

Observed, highly resolved surface data (surface pressure and temperature) from 96 meteorological stations in Germany were available. We purchased these data from DWD (Deutscher Wetterdienst). These data span from January 1, 2004 to December 31, 2007, with a time step of 10 min.

As a preliminary step, these DWD data were checked (removal of outliers; interpolation of small gaps). Then they were interpolated to a regular latitude/longitude grid using the MINC algorithm (Minimum Curvature, i.e., splines).

Using these grids, atmospheric corrections for the stations MO and BH were computed. This was done according to the method proposed by Merriam (Merriam 1992). In the calculation of the Newtonian attraction part a vertical pressure and temperature distribution is used which is based on a model atmosphere together with the pressure and temperature values at the Earth's surface. For the deformation part, Green's functions are used (Farrell 1972). These reductions were applied to the gravity residuals and compared to the standard reduction (using a regression coefficient (admittance) computed between local air pressure and gravity, cf. Torge 1989, Melchior 1983).
The deformation part of the Merriam correction was calculated using sea-level pressure (SLP), which was obtained from surface pressure and temperature via the barometric height formula. We included the Merriam temperature correction part; this cannot be neglected.
After the Merriam correction (and also after the 3D correction in Chapter 4), a regression was applied between the gravity residuals and the local station air pressure, and the result was subtracted from the gravity residuals. However, this procedure has little effect on the resulting final gravity residuals and their RMS. (The coefficient of correlation between the 2D corrected residuals and the local air pressure is near +0.20 … +0.25, depending on the station [Moxa or Bad Homburg] and on the time interval considered.)

4. Usage of 3D data

The 3D atmospheric fields used were obtained from the Institute for Meteorology and Climate Research (IMK-IFU) in Garmisch-Partenkirchen which is a branch of the KIT (Karlsruhe Institute of Technology). They were computed in a high resolution simulation with the WRF-ARW model (The Weather Research and Forecast Model, Skamarock et al. 2008). These data are given on a big 'square' over all of Europe with a horizontal resolution of 10x10 km^2. In the vertical, they consist of 41 layers up to about 28 km altitude. The data were provided with a temporal resolution of 1 h and they cover the time interval from January 1 to June 30, 2006. Due to the computational demand, only a single configuration of the atmospheric model could be exercised within the presented study. The setup consisted of version 3.1.1 of the WRF-ARW model and physics selected as follows: WSM 5-class microphysics, RRTM long-wave and Goddard short-wave radiation, YSU PBL scheme, NOAH land surface model, and Kain-Fritsch convective parametrization.
The computation of the 3D atmospheric correction was done using a given C++ program that had been created at GFZ Potsdam as part of a Diploma thesis (Stöber 2005). This software tool was adapted to the present 3D data. It calculates both the attraction and the deformation part.

For the attraction part, we used spherical volume elements for which a closed expression exists involving square roots and logarithms (Neumeyer et al. 2004, 2006).

It is first necessary to transform the 3D data (1.1 TByte) from the 'Lambert conformal conic projection' to a regular latitude/longitude grid. We chose grid cells of 0.10°x0.10°.

The following data variables were used in the computation of the 3D atmospheric correction:

- density of air (3D),
- geopotential (3D),
- surface pressure (2D),
- topography (2D) [which is smoothed to 10 km],
- land-ocean-mask (2D)

For the 3D calculations, the geopotential at the Earth's surface (lowest level) was constructed as: i) equal to zero over the oceans;
ii) from the height of the topography over land.

Furthermore, the deformation part was computed using the surface pressure instead of the sea-level pressure, because sea-level pressure (or surface temperature) data were not available for a temporal resolution of 1 h.

As the 3D data go up to an altitude of about 28 km only, we appended an extrapolated Standard Atmosphere (for mean latitudes) above 28 km up to 60 km altitude.

5. Description of the results and discussion

Both atmospheric reduction methods as discussed above (2D and 3D) were applied to the gravity residuals for MO and BH, and the results were compared among each other and with the standard reduction method.

Fig. 1 shows the 2D-correction (Merriam method, upper plot) for the station Moxa compared to the standard pressure correction and compared to the 3D-method (lower plot). From this Figure, we can deduce:

- The calculated 2D- and 3D-corrections have almost the same temporal behavior as the standard correction method.
- The 2D-reduction (upper plot) has only very small deviations from the standard reduction method. However, there are relatively large deviations between the 3D- and 2D-method (lower plot, e.g., at ~60.000 min and ~220.000 min). For some time intervals, the 3D-correction looks 'like a smoothed version' of the 2D-correction.

The differences between the three methods are more clearly visible after the application of the atmospheric correction to the gravity residuals. This is shown in **Fig. 2** for both SG-stations. In this Figure, the gravity residuals of Moxa and Bad Homburg are compared after applying an

atmospheric correction according to the three methods (standard pressure correction, 2D method after Merriam and 3D correction). From the plots for both stations, we can infer:

- The temporal behavior of the 2D atmospheric correction (Merriam method, green curve) is in a good agreement with the standard air pressure correction (red curve). However, it's obvious that the 2D method gives a significantly higher noise (c.f. the red and green curves in Fig. 2 for Moxa and Bad Homburg). This finding is also reflected by the RMS values of the residuals (for example: Moxa: 5.5 nm/s^2 for the standard air pressure correction versus 6.05 nm/s^2 for the 2D-correction).
- The remaining residuals after the application of the 3D atmospheric correction show a significantly different behavior compared to the 2D-correction and the standard air pressure correction. Please note particularly the positive and negative 'spikes' near ~100.000 min und ~170.000 min for both stations.
- From a comparison with other meteorological information, we found out that the strong 'spike' near ~100.000 min took place when a front passed and air pressure increased suddenly. The 'spike' caused by the application of the 3D atmospheric correction is an indication that short-time pressure rises are not yet correctly modeled in the underlying WRF model 3D data.

The **Figures 3** and **4** show the PSD (Power Spectral Density) of the gravity residuals from Fig. 2. Here, we only plotted the spectra from the 3D method compared to the standard method, both for Moxa (Fig. 3) and Bad Homburg (Fig. 4). Two plots are shown for each station with different frequency axes: linear (bottom) and logarithmic (top). The corresponding spectra for the 2D atmospheric correction are not shown here, because they are not significantly different from the standard method.

From **Fig. 3** and **4** we conclude:

- It's clearly visible that the spectra for the 3D atmospheric correction have a higher spectral power than those for the standard reduction method. This means that the application of the 3D atmospheric correction caused a rising of the noise level in the final gravity residuals.
- Both spectra (using 3D- and standard air pressure correction) contain the same peaks near higher harmonics of the diurnal variation (frequencies: 1/d, 2/d, 3/d).

Comparing the reduction results, we come to the following conclusions:

1. The **Merriam method** by using **2D data** from DWD produced a small increase in the noise of the gravity residuals compared to the standard method. The reasons for this finding could be:

   - There are parts in the atmosphere which do not correlate with the meteorological variations at the Earth's surface. These parts have a stronger influence than assumed,

   - Effects from the near surrounding area (some 10 km around the gravimeter) have a stronger influence than assumed; that means a very fine observation mesh would be necessary for significant improvements in the future.

2. The temporal behavior of the 3D correction differs more strongly from the standard air pressure correction than the 2D Merriam method. In particular the applied 3D correction

produces some incorrect 'spikes'. This indicates that the present quality of the 3D data is not yet sufficient to give an improvement in the atmospheric reduction of gravity time series compared to the standard air pressure method. Nevertheless, one should have in mind that only an individual realization of a high resolution atmospheric model was applied. Different configurations of WRF-ARW are known to yield different results, in particular with respect to the moisture budgets (Fersch et al. 2009). Additional comparisons with alternative setups should be tested in order to investigate possible variations. For instance, in contrast to other models, the selected configuration of the WRF-ARW model explicitly considered the humidity of air, but this is obviously not sufficient for an improvement in the atmospheric reduction.

Our conclusion is that the standard air pressure reduction (admittance coefficient) is presently still the most effective reduction method in the short-period spectral range, although this method produces some small errors near the higher diurnal harmonics, because of the global character of pressure variations near these periods.

Investigations by Gebauer et al. (not yet published) within the DFG-project KR1906/7-1 have shown that the deformations of the crust at a typical SG location are caused to 98% by the structure of the loading field at every observation time. Maximally 2% of the effects are caused by topography and crustal heterogeneity. This result (as well as the insights concerning the strength of the attraction effect in the zone of some 10 km around the gravimeter) clearly imply that the strategy of higher temporally and spatially resolved meteorological data must be pursued further. It seems that the available meteorological data sets are not yet sufficient in the short period spectral range. One option to overcome this drawback exemplarily could be the installation of a high resolution meteorological observation net around a dedicated SG station. There are efforts in this direction, but from our knowledge a high resolution 2D observation net has not yet been established. The registration of the vertical atmospheric variations above an SG site is an open question. One option could be the usage of atmospheric variation measurements derived from GPS observations at the SG location.

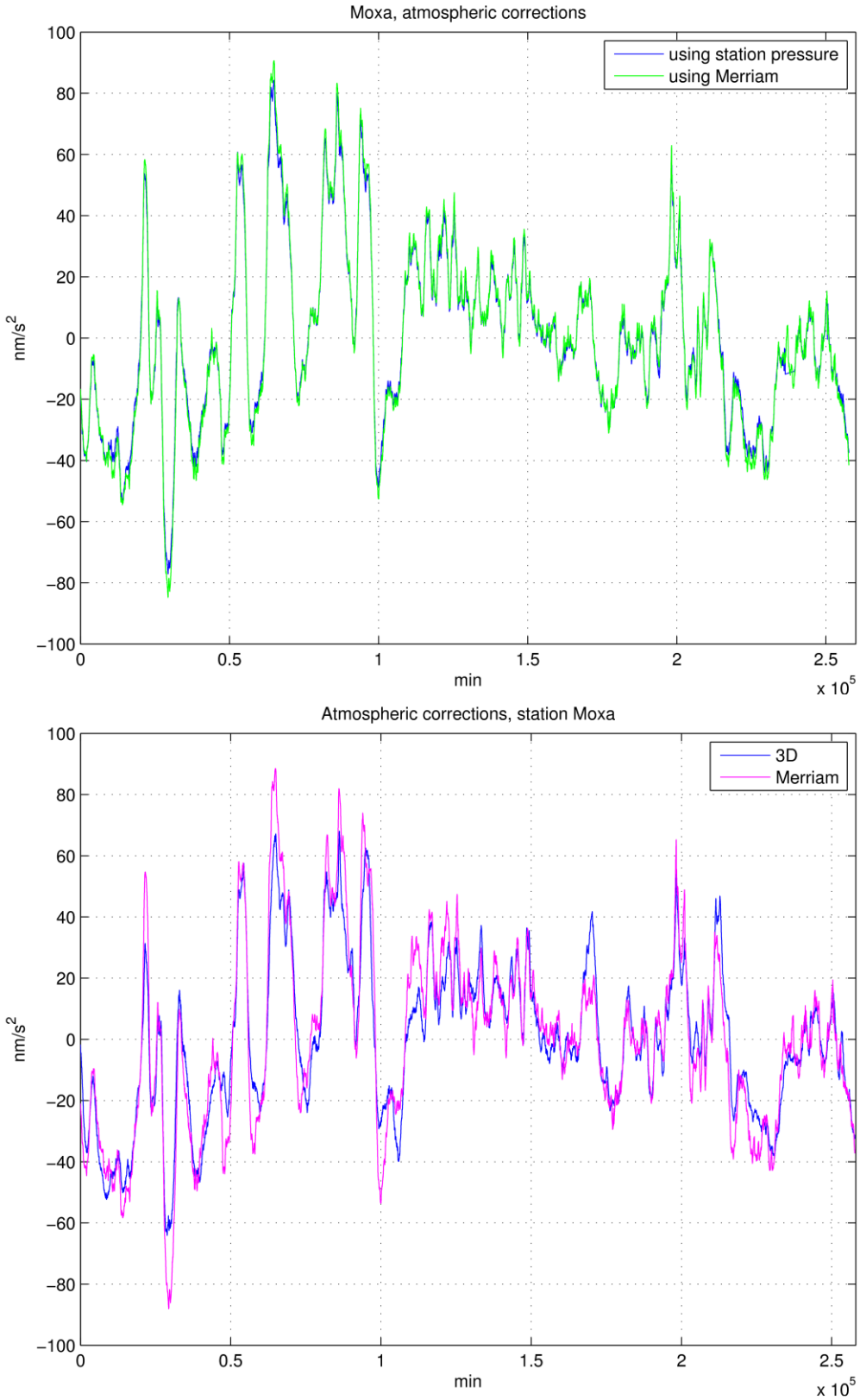

Fig. 1: Atmospheric corrections at the SG station Moxa from the 2D-data (method of Merriam) compared to the standard air pressure correction (upper plot) and compared to the 3D-method (lower plot). The time axis is given in [min] since January 1, 2006.

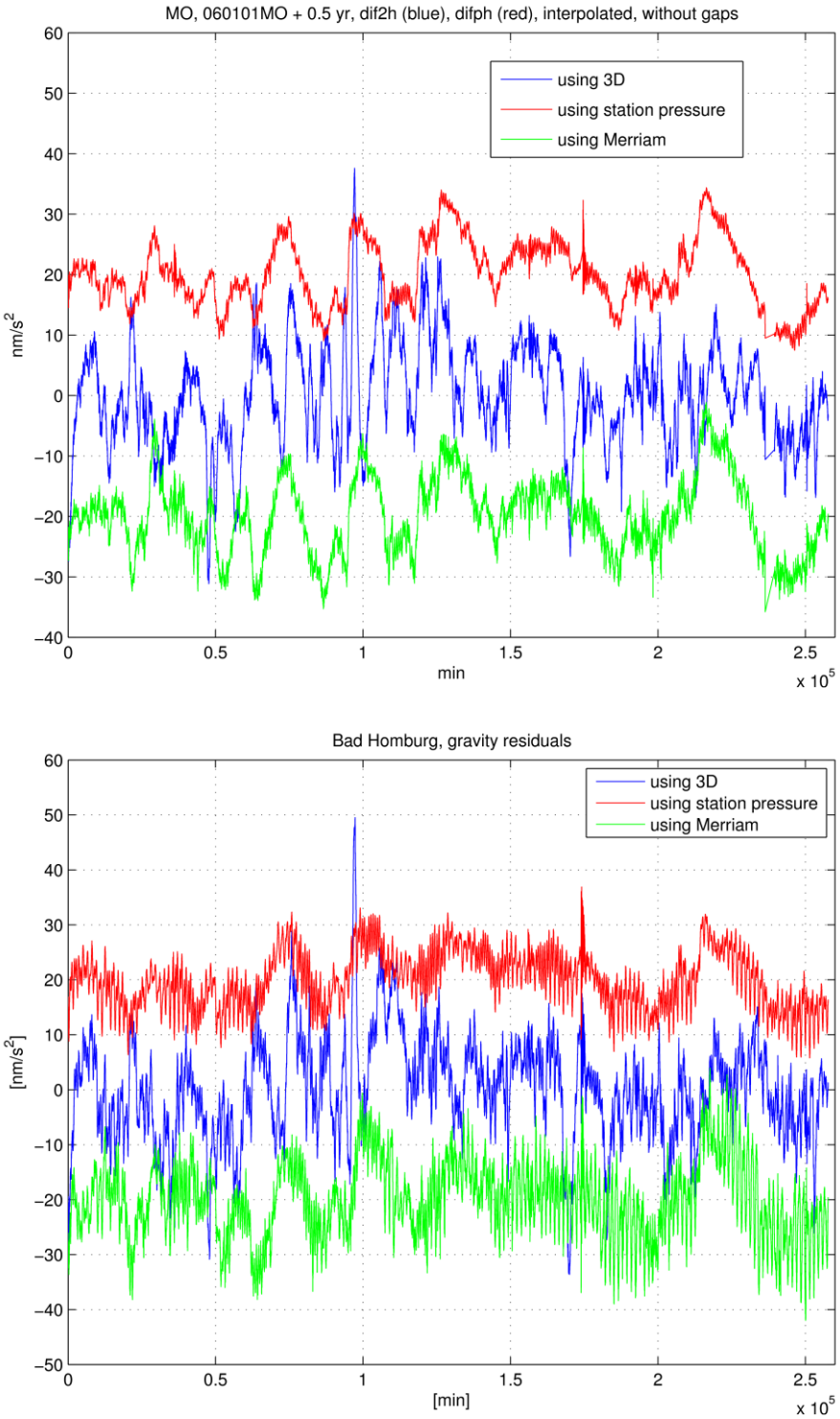

Fig. 2: Gravity residuals for the stations Moxa (upper plot) and Bad Homburg (lower plot) when using the standard air pressure correction (red), the 3D-correction (blue) and the Merriam-correction (green) for the time interval January 1, 2006 to June 30, 2006. Please note, that constant offsets have been added to the red and green curves compared to the blue curves.

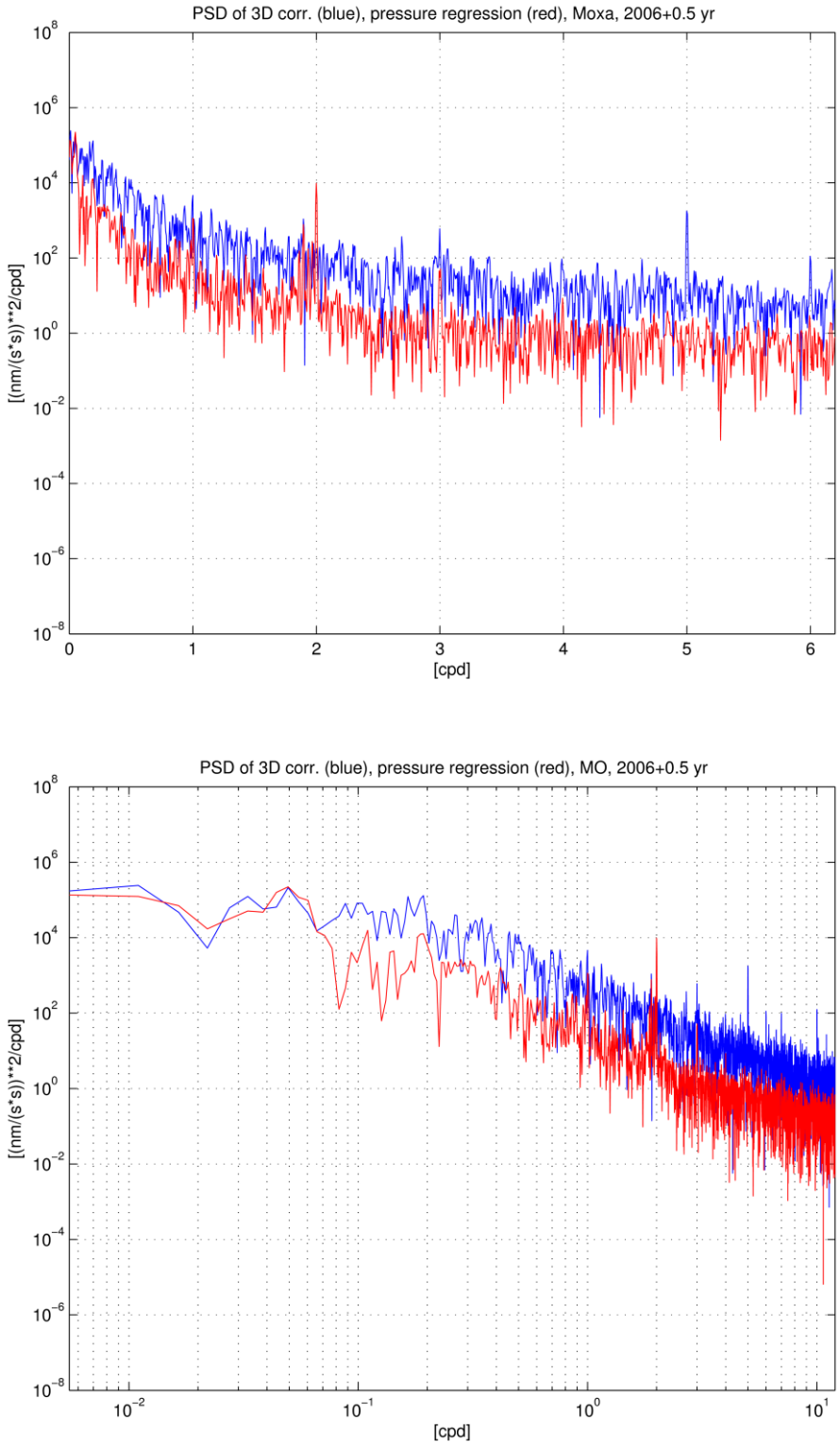

Fig. 3: Power Spectral Density (PSD) of the gravity residuals at the SG station Moxa for the 3D-method (blue) and the standard air pressure correction method (red), with linear (upper plot) and logarithmic frequency axis (lower plot).

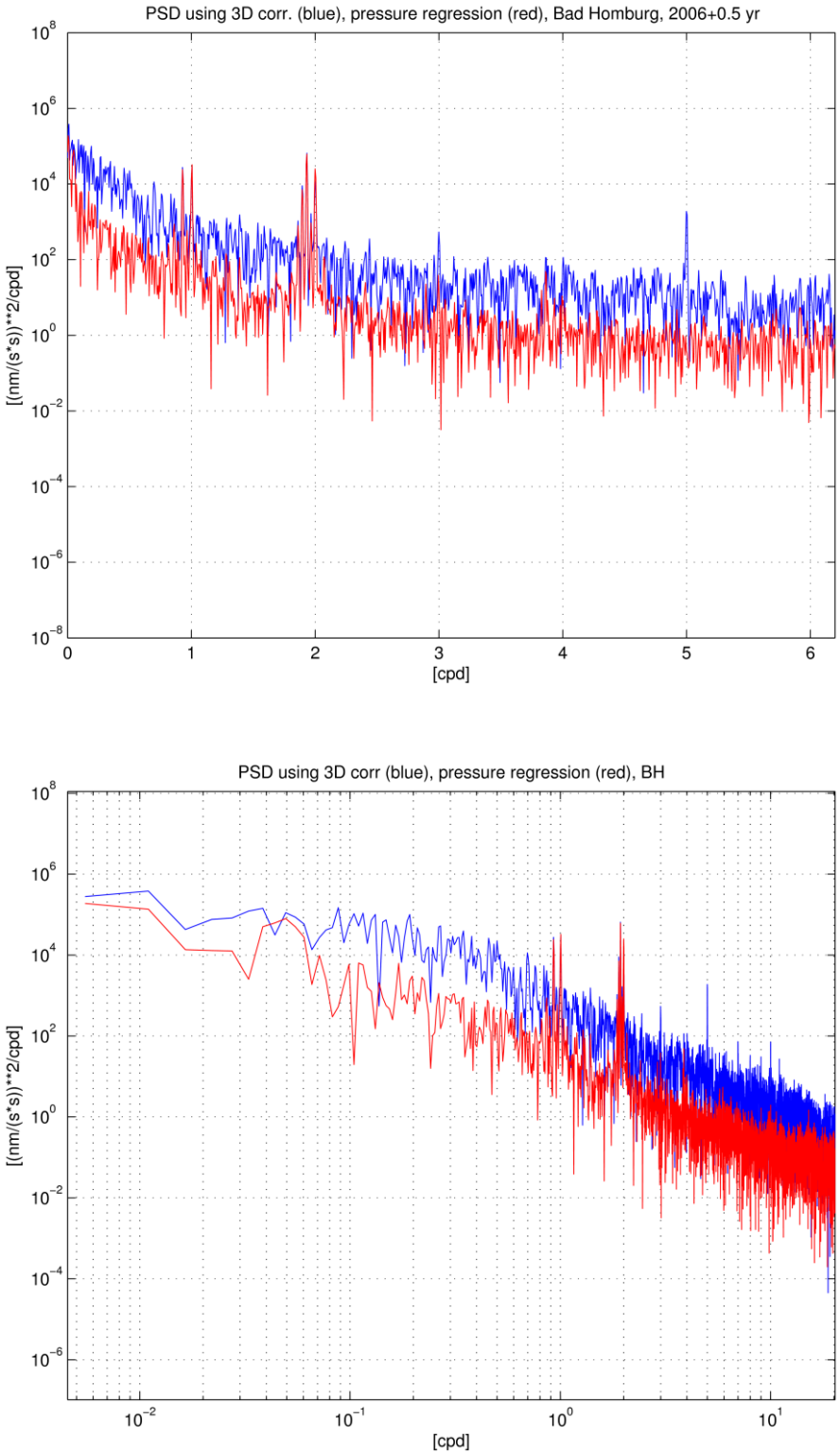

Fig. 4: Power Spectral Density (PSD) of the gravity residuals at the SG station Bad Homburg for the 3D-method (blue) and the standard air pressure correction method (red), with linear (upper plot) and logarithmic frequency axis (lower plot).

Acknowledgements: This study has been funded by the Deutsche Forschungsgemeinschaft (DFG) as third party funded project (DFG reference number KR 1906/14-1). Furthermore, we thank M. Abe and S. Petrovic (both at GFZ Potsdam) for discussions. P. Lehmann (Univ. of Jena) gave support with the data preparation. For interpolating the 3D data, we used CDO (Climate Data Operators) from Max Planck Institute for Meteorology, Hamburg.

References:

Abe, M., Kroner, C., Neumeyer, J., Chen, X.D., 2010. Assessment of atmospheric reductions for terrestrial gravity observations. Bull. d'Inf. Marées Terr., 146, 11817-11838.

Creutzfeldt, B., Güntner, A., Thoss, H., Merz, B., Wziontek, H., 2010. Measuring the effect of local water storage changes on in situ gravity observations: Case study of the Geodetic Observatory Wettzell, Germany. Water Resources Research, 46, W08531, doi:10.1029/2009WR008359.

Dobslaw, H., Thomas, M., 2007. Simulation and observation of global ocean mass anomalies. J. Geophys. Res., 112, C05040, doi:10.1029/2006JC004035.

Farrell, W.E., 1972. Deformation of the earth by surface loads. Rev. Geophys., 10, 761-979.

Fersch, B., Kunstmann, H., Sneeuw, N., Devaraju, B., 2009. Large-scale water balance estimations through regional atmospheric moisture flux modeling and comparison to GRACE signals. New Approaches to Hydrological Prediction in Data-Sparse Regions. (Proc. of Symposium HS.2 at the Joint IAHS & IAH Convention, Hyderabad, India, September 2009), 211-219.

Klügel, T. and Wziontek, H., 2009. Correcting gravimeters and tiltmeters for atmospheric mass attraction using operational weather models. J. Geodynamics, 48, (3-5), 204-210, doi:10.1016/j.jog.2009.09.010.

Melchior, P., 1983. The tides of the planet Earth. Oxford, Pergamon Press.

Merriam, J. B., 1992. Atmospheric pressure and gravity. Geophys. J. Int., 109, 488-500.

Naujoks, M., Kroner, C., Weise, A., Jahr, T., Krause, P. and Eisner, S., 2010. Evaluating local hydrological modelling by temporal gravity observations and a gravimetric three-dimensional model. Geophys. J. Int., 182, 233-249.

Neumeyer, J., Hagedoorn, J., Leitloff, J. and Schmidt, T., 2004. Gravity reduction with three-dimensional atmospheric pressure data for precise ground gravity measurements. J. Geodynamics, 38, 437-450.

Neumeyer, J., Schmidt, T. and Stöber, C., 2006. Improved determination of the atmospheric attraction with 3D air density data and its reduction on ground gravity measurements. In: Dynamic Planet; IAG Symp., Cairns, Australia. P. Tregoning and Ch. Rizos, eds., IAG Symp. 130, 541-548. Berlin, Springer.

Rosat, S. and Hinderer, J., 2011. Noise Levels of Superconducting Gravimeters: Updated Comparison and Time Stability. Bull. Seismol. Soc. of America, 101, 1233-1241, doi:10.1785/0120100217.

Skamarock, W. C. et al., 2008. A Description of the Advanced Research WRF Version 3. NCAR/TN-475+STR, NCAR Technical Note, Boulder.

Stöber, C., 2005, Modellierung und Analyse des Einflusses der 3D-Luftdruckkorrektur in Supraleitgravimeter-Registrierungen auf die langperiodischen Gezeitenparameter, Diploma thesis, Technische Universität Berlin 2005, prepared at Deutsches GeoForschungsZentrum GFZ.

Torge, W., 1989. Gravimetry; Berlin, de Gruyter.

Primary results of new gravity station Shaki/Azerbaijan

Samir Mammadov[1] , Thomas Jahr[2], Gerhard Jentzsch[2], Fakhraddin Kadirov[1].

1 - Geology Institute, Azerbaijan National Academy of Sciences, Baku, Azerbaijan

2 - Institute of Geosciences, Friedrich Schiller University Jena, Burgweg 11, D-07749 Jena, Germany

Abstract

In this paper we discuss the first results of a gravity tidal record obtained with the new gravity meter manufactured by the company ZLS (Zero-Length-Spring Corp.). This is also the first record of this kind in a station in Azerbaijan. And we discuss the results with regard to the dynamics of the Earth-Moon system and the deformation of the Earth caused by tidal forces and regional contemporary movements and deformations.

The gravimeter is installed in the geodynamic station Shaki, Azerbaijan, operated by the Institute of Geology of the National Academy of Sciences of Azerbaijan. The data covers the period of 2010-2011 and was processed in the Institute of Geosciences, Friedrich-Schiller-University of Jena, Germany.

1. Introduction

The experimental data are important in the modelling of the tidal deformation to calculate the tidal corrections for high-precision measurements of gravity which, together with other high-precision geophysical measurements, will reflect the variable deformations and stress in the crust.

Strain is actively manifested at the boundaries of tectonic plates, in zones of contact platforms and seismic areas, in zones of deep faults of the crust. Information about long-term changes in displacement, gravity, deformation and tilt allows the evaluation of stresses in the Earth's crust to study the structure of the region and the connection with seismic activity (Balenko et al.1985; Pariyskiy et al. 1980; Hinderer & Crossley, 2000; Mantovani et al. 2005).

Observation of Earth tides is a promising method for geodynamic studies. Observation of different tidal components (tidal variations of gravity, tilt, linear and volumetric strains, ocean tides, etc.) make it possible to determine the amplitude- and phase-frequency characteristics of the different layers of the Earth, giving information on their viscoelastic properties in the range of nearly diurnal frequencies, and complement, thus, seismic results.

The highest accuracy is achieved in observations of tidal variations of gravity, but, compared to tilt and strain, they are less affected by anomalies in the crust and upper mantle.

Azerbaijan's territory is located in a zone of active collision of two continents, Africa and Eurasia (Mckenzie, 1972; Sengor et al., 1985; Philip et al., 1989; Kadirov et al., 2008).

Azerbaijan is part of the Alpine-Himalayan fold - erogenous zone. The main geomorphologic elements are the Large and the Lesser Caucasus, Talysh, Kura and South Caspian Basin. The modern structure of the region continues to be influenced by the opposing horizontal tectonic movements in the Arabian and Eurasian plates (Philip et al., 1989; Shevchenko et al., 1999; Khain, 2001; Jackson et al., 1992, Kadirov et al., 2008, and Ahmedbeyli, 2004).

Since Azerbaijan is located north of the north eastern (NE) corner of the Arabian plate, the horizontal movements of the plates cause strong deformations of the crust. Therefore, the territory of Azerbaijan is an inherent uneven location of seismic events.

Fig. 1 shows a map of GPS-derived site velocities within the territory of Azerbaijan in the context of selected GPS velocities in surrounding areas. Velocities are shown in an Eurasia-fixed reference frame determined by minimizing motions for GPS stations that have been observed well and are broadly distributed across the Eurasian plate.

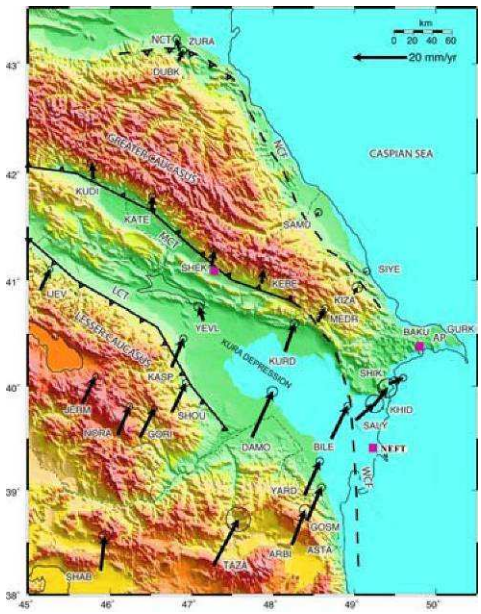

Figure 1. Azerbaijan GPS-Geodynamics Network. Triangles are survey sites and the square, the continuously recording GPS station at the Geology Institute, Baku. Base map shows topography, simplified tectonics. Abbreviations: NCT = North Caucasus Thrust fault, MCT = Main Caucasus Thrust fault, LCT = Lesser Caucasus Thrust fault, WCF = West Caspian Fault, NCF = North Caspian fault, AP = Absheron Peninsula (compiled by F. Kadirov, S. Mammadov, R. Reilinger, S. McClusky).

Velocity uncertainties are mostly less than 0.6 mm/yr, allowing fairly precise estimates of convergence across the Caucasus mountain system (i.e., uncertainties are about 5% of the total convergence rate; Kadirov at al., 2009; Reylinger at al., 2008). On a broad scale, the GPS velocity field clearly illustrates the NNE motion of Azerbaijan and adjacent regions of the Lesser Caucasus with respect to Eurasia south of the MCT. The most pronounced feature of the velocity field is the decrease in site velocities across the MCT.

2. Shaki station

Shaki station of the Institute of Geology of Azerbaijan National Academy of Sciences is located on the north-west of Azerbaijan (Fig. 2). In the foothills of the Greater Caucasus at a height of 723 m, and is the main Earth-tidal station in Azerbaijan. The station is located on the territory of Shaki Research Centre. Construction of the plant began in 2009. It consists of a separate room of 3m x 4m. In the middle of the room there is a concrete pillar of a size of 80cm x 80cm and a depth of 1.5 meters with a height above the ground of 65cm (Fig. 3).

The coordinates of the station are: 41.2220°N, 47.1710°E, elevation: 723.000 m.

Tidal measurements at the station Shaki began in March 2010. Excluding breaks in recording, the observations cover 358 days in a time span of little more than one year (01.04.2010 until 08.04.2011). We installed the automated Burris Gravity Meter B-14 (Adams et al., 2004; Jentzsch, 2008).

The Burris Gravity Meter™ is a product of the company ZLS Corporation, Austin/Texas, USA. It is based on the invention of L. LaCoste and A. Romberg (LaCoste, 1942): The zero length spring (ZLS).

Figure 2. Azerbaijan gravity station Shaki.

Figure 3. Azerbaijan gravity station Shaki.

The high-precision automated Burris gravimeter ensures accuracy in stationary observations to 0.1 microgal. The sensor type is a metal zero-length spring supported by a hardened metal micrometer screw with a range of 7,000 mGal. The feedback range is about ± 25 mGal, but can be reduced for Earth tidal purposes[1].

Particular attention was paid to ensure the temperature stability of the room. The temperature is kept constant throughout the year at around 2 to 3°C. In the winter and summer months, especially when large temperature differences occur, the gravimeter was covered by a special insulation.

[1] This gravimeter is mostly used for surveying and has demonstrated its superb quality (Ziang et al., 2012), some groups have provided continuous records (Poland & Carbone, 2010), using a WINDOWS based recording system now available which includes a digital barometer and a GPS time control. The data are stored on the hard disk of a notebook computer (www.gravity-consult.de).

3. Data analyses

Data processing and analysis was carried out in the Institute of Geosciences, Friedrich-Schiller-University of Jena, Germany. The observation results were processed using a combination of programs PreAnalyse (Gebauer et al., 2007) and ETERNA (Wenzel, 1996).

- Data acquisition system: For recording the data we used the program UltraGrav™ provided by ZLS with the control-computer HP200 palm-top. The HP200 employs the familiar DOS operating system. Data are stored on a PC memory card. This PC memory card is used like a floppy disk to transfer data from the HP200 to a host computer equipped with a PC memory card interface[2].
- Dynamic of recording: For long-term Earth tide (ET) observations and secular studies we are using the function "Continuous observations". This function permits the continuous measurement of gravity as required for Earth tide observations and secular gravity studies.
- Sample rate: The date sample rate was set to 3 minutes.
- Time base: Date and time were adjusted to UTC.
- Interpolation of gaps: During the primary treatment we introduced gaps where data were missing.
- Filtering: The 3min samples were interpolated to 1 Min., cleaned with PreAnalyse and filtered to 5min- and 1-hour-samples.
- Gaps in the data are associated with power failures.

As a result of the treatment a time series of hourly values was obtained (Fig. 4). A linear drift, superimposed by a seasonal period is clearly shown, in which the tidal amplitude is changing from about -100 nm/s² (10 µGal) to approx. -2000 nm/s² (-200 µGal). This drift rate is typical for spring gravimeters, even if they are specially constructed for the observation of Earth tides (Hegewald et al., 2011). Fortunately, there was only one bigger gap in the time series at the beginning of December 2010, due to power failure.

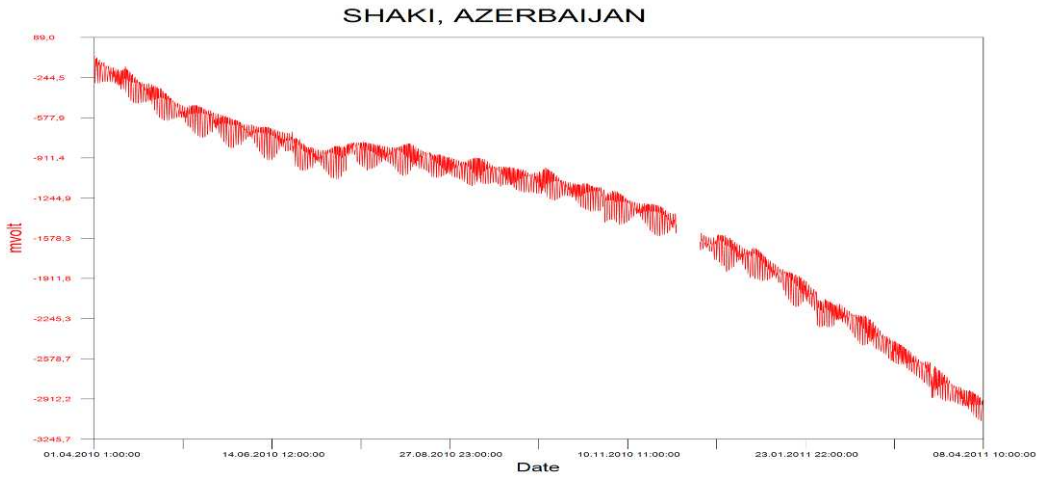

Figure 4. Tidal observation at station Shaki hourly values (calibration factor 1mvolt = 12.88 nm/s²)

We have computed the amplitude and phase spectrum of the hourly time series (Fig. 5: amplitude in nm/s²; phase in degrees, Fig. 6). The result shows clearly the diurnal and semi-diurnal tidal wave groups (Fig. 5). The long- and aperiodic drift behaviour shown in Fig. 4 can be seen in the lower frequencies of the spectrum, where the values rise up to some hundreds nm/s².

[2] See footnote 1.

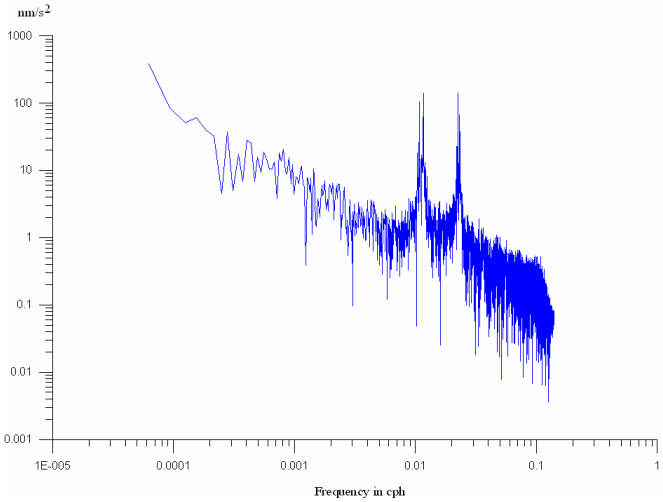

Figure 5. Amplitude spectrum in nm\s^2

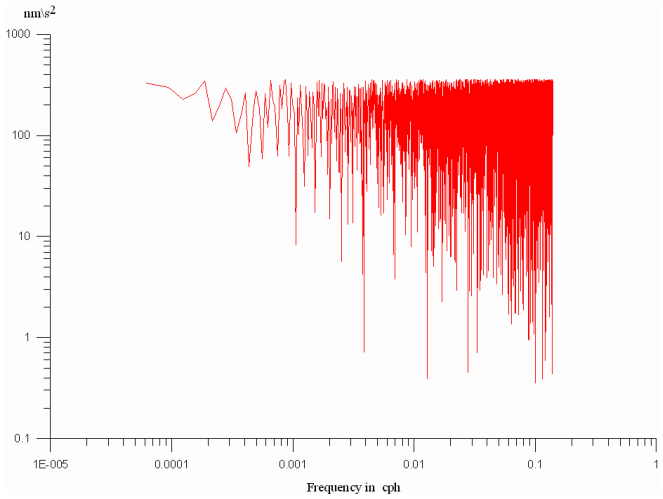

Figure 6. Phase spectrum in degrees.

4. Results – tidal parameters

The time series were analyzed using the tidal analysis program ETERNA3.4 (comp. Wenzel, 1997), and 18 main tidal constituents are used. Unfortunately, the barometric pressure could not be taken into account, because no parallel recording could be provided. The results with a standard deviation of 2.3nm/s² show the expected tidal parameters for an elastic Earth with a tidal factor of about 1.16 and phase differences close to zero for what concerns the main tidal constituents O1 and M2. The ocean tides loading is certainly not very large. S2 is clearly affected by the atmospheric pressure effects. The amplitude factor of M3 is close to the theoretical value 1.07 for the ter-diurnal waves. Only the tidal waves with very small amplitudes like J1, OO1 and also M4 show large errors or phase differences (Table 1).

The good quality of the tidal analysis is also confirmed by the tidal residuals (Fig. 8). The residuals mainly consist of white noise, however a seasonal variation can be seen. In autumn and winter time, at the end and at the beginning of the time series higher residuals of up to ± 10nm/s² are observed, whereas in summer time (mid of time series) the amplitudes vary by about ± 5nm/s² only. This is probably caused by the effect of barometric pressure variations, which usually show higher amplitudes in winter than in summer time.

Table 1. Adjusted tidal parameters estimated by the tidal analysis (ETERNA3.4).

From [cpd]	To [cpd]	wave	amplitude nm/s^2	amplitude factor	Standard deviation	phase lead [deg]	Standard deviation [deg]
0.501370	0.911390	Q1	66.94	1.135	0.008	1.84	0.43
0.911391	0.947991	O1	354.57	1.151	0.002	0.96	0.08
0.947992	0.981854	M1	28.23	1.166	0.016	-0.41	0.78
0.981855	0.998631	P1	161.07	1.124	0.004	-0.55	0.19
0.998632	1.001369	S1	17.58	5.194	0.229	77.60	2.53
1.001370	1.004107	K1	489.74	1.131	0.001	1.18	0.06
1.004108	1.006845	PSI1	10.76	3.176	0.155	-8.09	2.80
1.006846	1.023622	PHI1	8.77	1.422	0.087	20.12	3.50
1.0236230	1.057485	J1	26.88	1.110	0.021	7.41	1.11
1.057486	1.470243	OO1	15.09	1.139	0.030	5.25	1.51
1.470244	1.880264	2N2	15.61	1.201	0.031	8.62	1.47
1.880265	1.914128	N2	95.78	1.177	0.006	1.83	0.31
1.914129	1.950419	M2	498.03	1.171	0.001	1.30	0.06
1.950420	1.984282	L2	13.90	1.157	0.051	-6.19	2.55
1.984283	2.002736	S2	229.43	1.160	0.003	0.61	0.13
2.002737	2.451943	K2	60.62	1.128	0.009	2.81	0.47
2.451944	3.381478	M3	6.79	1.079	0.077	1.08	4.10
3.381379	4.347615	M4	0.63	7.322	5.476	57.38	42.85

The tidal analysis also shows the well known *Nearly Diurnal Free Wobble* (NDFW) of the Earth, which is caused by the forced oscillation of the Earth core (Zürn, 1997). If the quality of the gravity time series is high enough this geodynamic effect can be detected in the diurnal frequency band: The tidal parameters of small constituents of PHI1 and PS1 should be higher than 1.16 and for the main constituent K1 should be slightly reduced compared to O1. Fig. 9 shows these parameters over the time in hours, and it is obvious that the NDFW was significantly observed by the gravity record in Shaki-station.

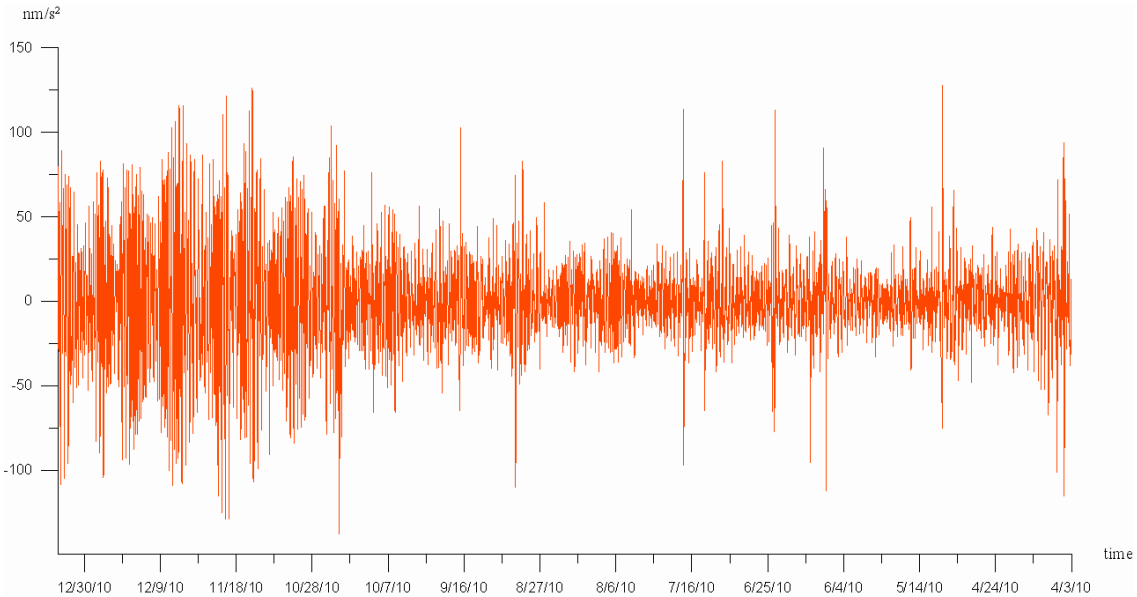

Figure 8. Tidal residuals after tidal analysis (ETERNA3.4).

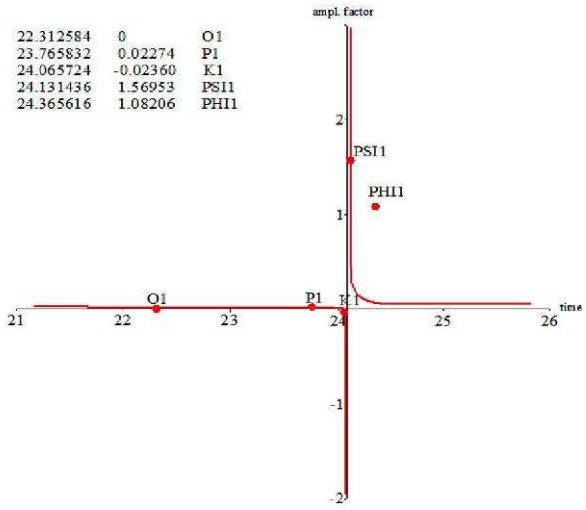

Figure 9. Nearly diurnal free wobble, caused by the Earth core is clearly indicated by the gravity observation in Shaki station.

5. Results – monthly analyses

The record was analyzed piecewise using moving windows of three months length each, moved by one month. Thus, the results were allocated to the middle centre month of the intervals. Tables 2 and 3 give the obtained results for amplitude factor and phase lead; Figures 9 and 10 give the plots of these results. Applying the errors obtained, in the semidiurnal tidal band the variations are not significant, whereas in the diurnal tidal band in some cases the error bars do not overlap. Especially in the case of the phase it seems to be strange, that all results show decreasing phases towards the end of the recording period. The fact the phase shift of M2 is nearly twice the phase shift of O1 points obviously to a timing error due to the drift of the clock.

Table 2. Amplitude factor: Monthly results for the main tidal waves O1, P1S1K1, M2, and S2, estimated by tidal analysis (ETERNA3.4).

Date	O1	P1S1K1	M2	S2
May	1.146 ± 0.005	1.138 ± 0.003	1.168 ± 0.002	1.163 ± 0.005
June	1.148 ± 0.005	1.129 ± 0.003	1.168 ± 0.002	1.157 ± 0.004
July	1.147 ± 0.005	1.116 ± 0.003	1.168 ± 0.001	1.173 ± 0.004
August	1.158 ± 0.004	1.114 ± 0.003	1.169 ± 0.002	1.165 ± 0.004
September	1.151 ± 0.003	1.102 ± 0.003	1.171 0.0014	1.178 ± 0.005
October	1.154 ± 0.003	1.117 ± 0.002	1.172 ± 0.001	1.181 ± 0.004
November	1.157 ± 0.004	1.116 ± 0.002	1.172 ± 0.004	1.168 ± 0.008
December	1.142 ± 0.005	1.122 ± 0.003	1.169 ± 0.003	1.199 ± 0.009

6. Conclusions

For the first time, a Burris gravimeter was used for tidal recording for a period of a little over one year. The results show that the gravimeter is stable and very well suited for such a purpose. Although the data quality is not as good as it could be due to the recording with a palm top, we are quite satisfied with the results. Compared to the environmental conditions the drift is quite tolerable and in accordance with other findings related to spring gravimeters. We hope to further improve the recording by replacing the palm top by a recording system with higher resolution, GPS time receiver and digital barometer to be provided by Gravity Consult GmbH.

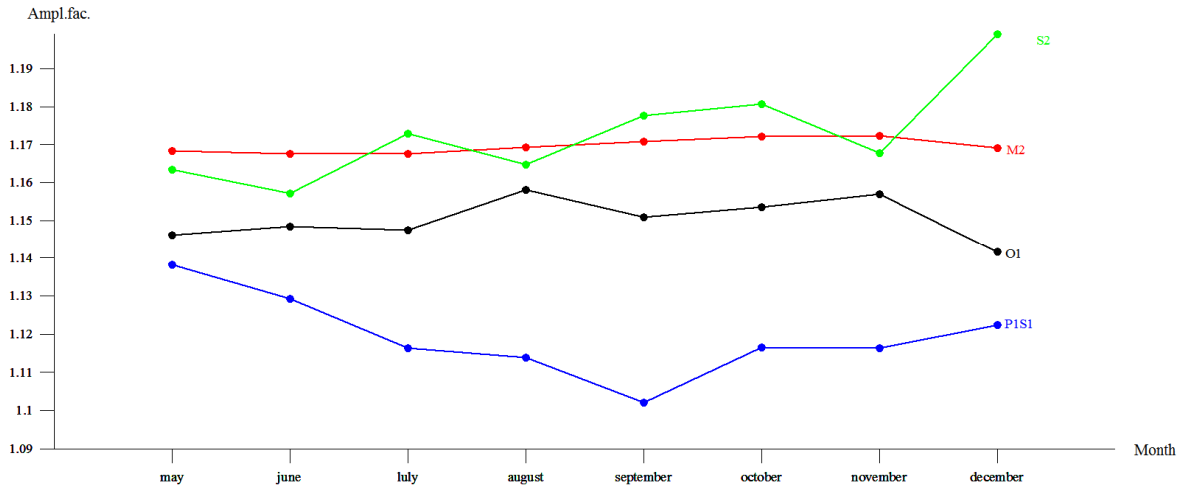

Figure 9. Amplitude factor: Monthly results for the main waves O1, P1S1K1, M2, and S2 estimated by tidal analysis (ETERNA3.4).

Table 3. Phase lead: Monthly results for the main waves O1, P1S1K1, M2, and S2 estimated by tidal analysis (ETERNA3.4).

Date	O1	P1S1K1	M2	S2
May	0.68 ± 0.25	0.56 ± 0.16	1.61 ± 0.09	0.77 ± 0.26
June	0.68 ± 0.25	0.52 ± 0.15	1.39 ± 0.08	-0.35 ± 0.22
July	0.73 ± 0.23	0.42 ± 0.15	0.84 ± 0.07	-0.12 ± 0.18
August	0.50 ± 0.21	0.18 ± 0.16	0.35 ± 0.09	-0.78 ± 0.21
September	0.08 ± 0.17	0.50 ± 0.15	-0.08 ± 0.07	-1.20 ± 0.22
October	-0.19 ± 0.15	1.39 ± 0.12	-0.59 ± 0.06	-2.40 ± 0.21
November	-0.65 ± 0.18	1.10 ± 0.12	-1.57 ± 0.13	-2.51 ± 0.38
December	-2.01 ± 0.24	-0.04 ± 0.14	-3.71 ± 0.14	-6.32 ± 0.42

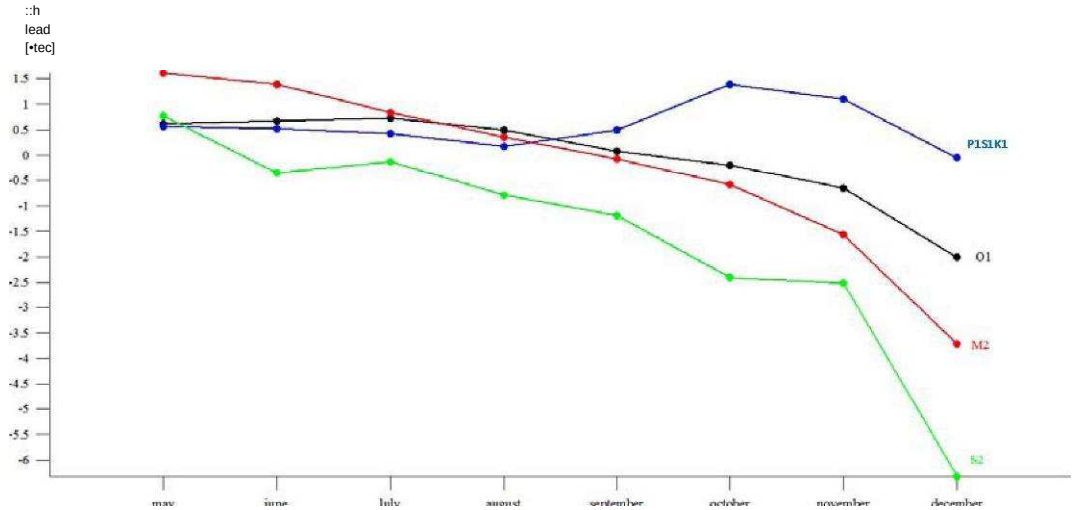

Figure 10. Phase lead: Monthly results for the main tidal waves O1, P1S1K1, M2, and S2 estimated by tidal analysis (ETERNA3.4).

7. Acknowledgements

This paper was mainly written during the work of Samir Mammadov within a postdoctoral fellowship at the Institute of Geosciences, University of Jena, Germany. We are thankful to the National Academy of Sciences, Baku, for funding this stay in Jena. The agreement of the German institute for providing working space is greatly appreciated.

Thanks to Bernard Ducarme for his comments to improve the manuscript!

8. References

Adams, J., L. Burris, G. Jentzsch, A. Kopaev, and H. Valliant, 2004. The Automated Burris Gravity Meter - a New Instrument for Surveying and Continuous Operation. 15th Int. Symp. Earth Tides, Ottawa, August 2004, Abstract Book.

Ahmedbeyli F.S., Qasanov A.Q., Kadirov F.A., Kadyrov A.H., Rzayev A.Q., Yetirmishly Q.D., Mammadov S.K., Quseynova V.P., 2004. Distribution of earthquake epicenters and seismic energy released in the territory of Azerbaijan (tectonic aspects, and some patterns). Catalogue of earthquakes, of the Republican Center of Seismological service of Azerbaijan National Academy of Sciences, Baku, pp.137-150.

Balenko I.Q., Barsenkov S.N., Bulancev V.Q., Qrideev D.Q., Dichenko I.A., Saricheva Y.K., Timofeev V.Y., 1985. Tidal gravity measurements in Novosibirsk in 1977-1979. Slowly deformation of Earth and its rotation. Moscow journal Radio and communication, pp. 40-59.

Gebauer, A., T. Jahr, and G. Jentzsch, 2007. Recording and interpretation/analysis of tilt signals with five ASKANIA borehole tiltmeters at the KTB. Review of Scientific Instruments, Vol.78, No.5.

Hegewald, A., G. Jentzsch, and T. Jahr, 2011. Influence of temperature variations on the noise level of the data of the LaCoste & Romberg Earth Tide gravity meter ET18. G-cubed, Vol. 12, No. 4, 8 pp, doi:10.1029/2010GC003432.

Jiang Z., Pблinkбљ V., Francis O., Jousset P., Mдkinen J., Merlet S., Becker M., Coulomb A., Kessler-Schulz K., Schulz H., Rothleitner Ch., Tisserand L., Lequin D., 2012. Relative Gravity Measurement Campaign during the 8th International Comparison of Absolute Gravimeters (2009). Metrologia.

Jackson, J., 1992. Partitioning of strike-slip and convergent motion between Eurasia and Arabia in eastern Turkey. J. Geophys. Res., 97, pp. 12471-12479.

Jentzsch, G., 2008. The automated Burris gravity meter – a new instrument using an old principle. Proc. Symposium on Terrestrial Gravimetry: Static and Mobile Measurements, St. Petersburg, Russia, 20-23 Aug. 2007, pp. 21-28.

Hinderer, J. and Crossley, D., 2000. Time variations in gravity and inferences on the Earth's structure and dynamics, Surv. Geophys., 21, pp. 1-45.

Kadirov, F. Mammadov, S., Reylinger. R., McClusky, S., 2008. Some new data on modern tectonic deformation and active faulting in Azerbaijan (according to Global Positioning System measurements). J. Proceeding the Sciences of Earth, Azerbaijan National Academy of Sciences, №1, pp. 83-88.

Kadirov F.A., Kadirov A.H., Aliye F.A., Mammadov S.K.,Safarov R.T., 2009. Correlation between speeds of horizontal movements defined on GPS to measurements in Azerbaijan and seismicity of the Create Caucasus. Catalogue of the seismoforecasting research carried out of Azerbaijan territory in 2008. Republican Survey Seismic Center of Azerbaijan National Academy of Sciences, pp. 121-126.

Khain V.E., 2001. Tectonics of continents and oceans, Moscow, Book, The scientific world, 606 pp.

LaCoste, 1942. US Patent 2293437. Cited after: Larson, J.V., (1968), A cross correlation study of the noise performance of electrostatically controlled LaCoste and Romberg gravimeters. Technical Report No. 752, University of Maryland, Dept. of Physics and Astronomy, College Park, Maryland.

Mantovani, M.S.M., Shukowsky, W., de Freitas, S.R.C., Brito Neves, B.B., 2005. Lithosphere mechanical behaviour inferred from tidal gravity anomalies: a comparison of Africa and South America. Earth Planet Sci. Lett. 230, pp. 397-412.

McKenzie, D.P., 1972. Active tectonics of the Mediterranean region, Geophys. J. R. Astron. Soc., 30, pp. 239-243.

Pariyskiy, N.P., Barsenkov, S.N., Volkov, V.F., Qridnev, D.Q., Kuyznetsov, L.V., Percev, B.P., Saricheva, Y.K., Varqa, P., Shimon, E., 1980. Tidal gravity variation in the USSR. Study of earth tides, Moscow. Science, pp. 65-84.

Philip, H., A. Cisternas, A. Gvisiani, and A. Gorshkov, 1989. The Caucasus: An actual example of the initial stages of continental collision, Tectonophysics, 161, pp. 1-21.

Poland, M.P., and D. Carbone, 2010. First results from continuous gravity measurements at Kilauea Volcano, Hawai'i. Poster G23C-0833, AGU Fall Meeting, San Francisco, December 2010.

Sengor, A.M.C., N. Gorur, and F. Saroglu, 1985. Strike-slip faulting and related basin formation in zones of tectonic escape: Turkey as a case study. In: Biddle, K.T. and N. Christie-Beck, (eds.) Strike-slip Faulting and Basin Formation, Society of Econ. Paleont. Min. Sec. Pub., 37, pp. 227-264.

Shevchenko, V.I., Quseva, T.V., Lukk, A.A. et al., 1999. Modern geodynamics of Caucasus by results of GPS measurements and seismological data. J. Physics of the Earth, №9, Moscow, pp.3-18.

Wenzel, H.-G., 1996. The nanogal software: Earth tide data processing package ETERNA 3.30. Bull. D'Inf. Marйes Terr., 124, pp. 9425 – 9439.

Zürn, W., 1997. The nearly diurnal free wobble-resonance. In: Wilhelm, H., W. Zьrn, and H.-G. Wenzel (Eds.), 1997. Tidal Phenomena. Lecturer Notes in Earth Sciences, 66, pp. 95 – 109.

The K1 triplet: Can Lunar nodal waves contribute to the study of the Free Core Nutation (FCN)?

Bernard Ducarme
Catholic University of Louvain, Georges Lemaître Centre for Earth and Climate Research
bf.ducarme@gmail.com

ABSTRACT

The longest series of superconducting gravimeters participating to the Global Geodynamics Project (GGP, Crossley et al., 1999) are now ranging between 10 and 18 years. It was possible to extract successfully the nodal waves for 12 series longer than 3,500 days using the VAV04 tidal analysis program (Venedikov and Vieira, 2004). In most of the cases the tidal parameters of the nodal waves agree with those of the main tidal constituent. The K1 triplet is especially interesting, being submitted to the resonance of the liquid core of the Earth. The amplitude factors of the three constituents should differ by 0.1% according to different Earth models. This effect is clearly seen in our results. We introduce a parameter $\rho\pm = |1- \delta_{K1}\pm/\delta_{K1})|$, free from calibration errors and ocean tides loading influence, to express the relative difference between K1 and its nodal companions $K1^-$ or $K1^+$. The $K1^-$ nodal wave has a too small amplitude to provide reliable results but the mean relative difference ρ^+ between K1 and $K1^+$ (0.113%±0.022%) is very close to the values 0.124% and 0.116% predicted respectively by the DDW99NH (Dehant et al., 1999) and the MAT01NH (Mathews, 2001) non hydrostatic models.

Keywords: superconducting gravimetry, Free Core Nutation, nodal waves

Foreword

The lunar nodal waves associated with the main tidal components have been fairly well separated from a 14 year long record of the superconducting gravimeter T003 (SG, Hinderer et al., 2007) of Brussels by Ducarme and Melchior (1998). The most interesting result concerned the K1 triplet associated with the 18.6124 year astronomical nutation. Fifteen year later most of the SGs operated since 1997 in the framework of the Global Geodynamics Program (GGP, Crossley et al., 1999) have records longer than 10 years that could be used for the same purpose.

1. Introduction

Let us consider the development of the tidal potential due to the Moon (Wenzel, 1997a)

$$W = \sum_2^\infty W_n = \frac{GM}{c}\sum_{n=2}^{\infty}(\frac{r}{c})^n \frac{1}{2n+1}\sum_{m=0}^{n} P_{nm}(\cos\theta).P_{nm}\cos(\pi/2-\delta).\cos(mH) \qquad (1)$$

with G gravitational constant, M mass of the Moon, r geocentric distance of the point of observation, c distance from the geocentre to the Moon, θ geocentric colatitude, δ declination of the Moon and H its hour angle. The P_{nm} are the fully normalized Legendre functions of degree n and order m. The order m is associated to the different tidal bands through the hour angle. The time variations of the potential are linked to r,δ and H. Expressing these quantities as a function of the astronomical arguments describing the motion of the celestial bodies inside the solar system, it is possible to develop the tidal potential in a sum of harmonic constituents, under the form

$$W = D\sum_{n=2}^{\max}\sum_{m=0}^{n}(\frac{r}{a})^n \Gamma_{nm}(\theta).P_{nm}(\cos\theta).\sum_i [C_i^{nm}\cos(\alpha_i t) + S_i^{nm}\sin(\alpha_i t)] \qquad (2)$$

with D [Newton.m], so called "Doodson constant", $\bar{a}$ mean equatorial radius, Γ_{nm} normalisation coefficients and $P_{nm}(\cos\theta)$ geodetic coefficients. The arguments α_i are expressed in function of astronomical arguments. If we consider only Moon and Sun, neglecting the planets of the solar system, we can write

$$\alpha_i = a\tau + bs + ch + dp + eN' + fp_s$$

with τ mean local lunar time (H+180°), s mean tropic longitude of the Moon, h mean tropic longitude of the Sun, p mean tropic longitude of the lunar perigee, N'=-N mean tropic longitude of the ascending lunar node changed of sign and p_s mean tropic longitude of the solar perigee. The angular speed of a tidal wave is completely determined by its argument under the form (a,b,c,d,e,f). Among the different development of the tidal potential one generally use as standards the TAM1200 potential (Tamura, 1987) and the HW95 catalogue (Hartmann and Wenzel, 1995).

From the tidal potential it is possible to compute the different tidal components. In this study we focus on the vertical component of the tidal force i.e. the variation of gravity. The Earth body submitted to the tidal forces is deformed and this deformation produces an additional change of potential. The global effect on the tidal gravity changes is characterized by the so called "amplitude factor". For a given tidal wave, the amplitude factor δ is defined as the ratio A/A_a (Melchior, 1983) of the effective amplitude A with respect to the astronomical tide of amplitude A_a. Several theoretical models of the Earth response to the tidal forces have been developed in the last decades: Wahr-Dehant-Zschau (Dehant, 1987), DDW99 (Dehant et al., 1999), MATH01 (Mathews, 2001). Their results provide the so called body tides with amplitude A_{th} and amplitude factor values $\delta_{th}= A_{th}/A_a$. It is thus possible to define the different body tides models by a vector $\mathbf{R}(\delta_{th}.A_a, 0)$, expressing the fact that the body tide is in phase with the astronomical one. The analysis of the observations will provide an observed tidal vector $\mathbf{A_o}(\delta A_a,\alpha)$, where α is the difference between the observed and the astronomical local phases with lag counted as negative. Unhappily it is generally not possible to compare directly the observed and body tides vectors as the ocean tides effect is still mixed up in the observations. The tidal loading vector **L**, which takes into account the direct attraction of the water masses, the flexion of the ground and the associated change of potential, is generally evaluated by performing a convolution integral between the ocean tide models and the load Green's function computed by Farrell (Farrell, 1972). We subtract the tidal loading effects $\mathbf{L}(L,\lambda)$ to get the so called "corrected" tidal parameters: amplitude factor δ_c and phase difference α_c.

$$\mathbf{A_c}(\delta_c A_a, \alpha_c) = \mathbf{A_o} - \mathbf{L} \qquad (3)$$

which can be directly compared with the body tides models **R**.

The Earth response is different for the different degrees of the potential. For W_2 the recent body tides models agree at the level of a few tenth of percent and these different models have been evaluated using tidal gravity observations, mainly superconducting gravimeters data provided by the GGP consortium. The DDW99 and MATH01 models agree with the observations corrected for the ocean tides loading at the level of 10^{-3} (Baker and Bos, 2003; Ducarme et al., 2001, 2002, 2007, 2009).

2. Constrains on the tidal analysis procedure

The analysis of earth tide observations is usually carried out by least squares adjustment. A general description of the procedure and of its advantages can be found for example in Wenzel 1997b. The goal of the tidal analysis is to determine the so called tidal parameters i.e. amplitude factors (ratio between the observed amplitude A_o and the theoretical one A_{th}) and phase differences (difference between the observed phase α_o and the theoretical one α_a), for

different tidal "wavegroups". The wavegroup concept was proposed by Venedikov (1961). Due to the limited resolution of any analysis technique, the frequency resolution is limited by the recording length T. According to the Rayleigh criterion the separation of the waves is generally restricted to $\Delta f \geq 1/T$. However the Rayleigh criterion should be used as a rule of thumb only. For the least squares adjustment method, where the frequencies are known beforehand, the separation depends on the recording length T and on the signal-to-noise ratio. For high signal to noise ratios, as it is the case with SGs, waves with frequency differences $\Delta f < 1/T$ can be sometimes separated. In any case it is impossible to determine individual tidal parameters for all the tidal waves contained in any tidal potential catalogue. Instead, average tidal parameters are determined for "wavegroups" containing neighbouring waves. The Rayleigh criterion applies in this case on the frequency difference between the main wave of two neighbouring wavegroups. It is supposed that the tidal parameters are identical for all the waves inside a wavegroup. This assumption is generally not verified as different degrees of the potential are mixed inside of the same group. To cope with this problem the usual practice is to multiply the theoretical amplitude of the waves which are not belonging to the same degree as the main wave of the group by the ratio of the theoretical amplitude factors. For example, if the tidal gravity factors for (2,2) and (3,2) terms in (2,2) group are δ_2 and δ_3 (Melchior, 1983), the theoretical amplitude of any (3,2) term will be multiplied by δ_3/δ_2. If the observed tidal factor of the group is δ, the contribution of a (3,2) term is in fact $\delta.\delta_3/\delta_2 \approx \delta_3$ if $\delta_2 \approx \delta$. This approximation is generally valid as the observed and theoretical tidal factors agree generally within a few per cent while the discrepancy between the theoretical factors of different degrees of the potential are of the order of 10%. Moreover the contribution of the components deriving from W_2 are much larger than the signal coming from the higher degrees of the potential, so that the residual effect becomes generally negligible. This procedure should be applied also to the terms generated by W_4.

3. First approach of the nodal waves

As a matter of fact the argument of the nodal waves differ only from the argument of their closest neighbour by the variable N' associated to the Lunar node, which has an angular speed of 0°.00220641 per hour. According to the Rayleigh criterion, the period required to separate such waves is thus 18.6124 years. In section 4 we discuss how it is possible to relax considerably this condition.

Let us consider first the data of the superconducting gravimeter CD021 at station Membach (BE). It is one of the longest and most precise series observed with a superconducting gravimeter (Hinderer et al., 2007) in the framework of the Global Geodynamics Project (GGP, Crossley et al., 1999). The Tables 1 and 2 present the characteristics of the principal nodal waves and the tidal factors computed with the ETERNA (Wenzel, 1996) software. It is noticed at the first glance that there do not generally exist a pair of nodal waves symmetrical with respect to the main tidal constituent. The exceptions are M1, K1 and NO1. NO1- (1,0,0,1,-1,0) with an amplitude of $0.7 nms^{-2}$ is not negligible, but it is located very close to M1+ (1,0,0,0,1,0), which has a similar amplitude (Table 2). The difference in angular speed is only p-2N' i.e. $2.29\ 10^{-4}$ deg/hour. The period of commensurability becomes then 179 years! We cannot separate both components simultaneously The separation of $M1^+$ becomes possible if we keep NO1 and NO1- in one and the same group. Inversely results for $NO1^-$ are obtained by grouping M1 and $M1^+$. However the precision is low.

In most of the cases the tidal parameters of the nodal waves agree with those of the main tidal constituent within one or two σ (RMS error). The main exceptions are P1 and K1 in the diurnal band, M2 in the semi-diurnal band and perhaps M3 in the ter-diurnal one. In the diurnal band the amplitude factors are frequency dependent due to the FCN resonance

(Ducarme et al., 2007). The slope of the resonance being steeper close to K1 and the nodal waves larger we can perhaps get some useful information on the FCN from the K1 triplet. Concerning M2 and M3 one can suspect a different resonance of the nodal waves with respect to the main tidal constituent in the ocean tides loading. However it is not confirmed by the analysis of the ocean tides records at Oostende (BE) between 1945 and 2006 as shown in Table 3.

4. K1 (1, 1, 0, 0, 0, 0) and its nodal waves $K1^-$ (1, 1, 0, 0,-1, 0) and $K1^+$ (1, 1, 0, 0, 1, 0)

As seen in the previous section, the K1 triplet (Table 1) is especially interesting, being submitted to the resonance of the liquid core of the Earth. The amplitude factors of the three constituents should differ by 0.1% according to different Earth models (Table 4). The GGP data base is incorporating the observations of 26 tidal gravity stations between 1997 and 2010. From the point of view of the Rayleigh criterion no series already reaches the 18.6124 year data length required for the separation of the nodal waves. Including data prior to GGP the series of Brussels (more than 18 years), Cantley (16.5 years) and Membach (14.5 years) hardly reach the required time span. Most of the stations however reach a data span larger than 10 year.

To save a maximum of series, we can use the advantages of the VAV04 tidal analysis program (Venedikov and Vieira, 2004). The main difference with respect to the more popular ETERNA software (Wenzel, 1996) resides in the filtering technique used to separate the tidal signal in the spectrum. ETERNA is applying overlapping high pass filters on the original data to produce filtered series still including all the complete tidal signal, while VAV04 is applying different odd and even filters to separate the tidal bands at different angular speed Ω: D (Ω=15°/h), SD (Ω=30°/h), TD (Ω=45°/h), QD (Ω=60°/h) and so on…. Moreover the filter length is generally limited to 48h and always applied without overlapping. The least square adjustment is applied on these discrete series of filtered data. The main advantage of VAV04 for the determination of the small nodal waves is the automatic elimination of noisy data (Venedikov and Ducarme, 2000) based on a statistical study of the residues of the filtered data in the four frequency bands: D (Ω=15°/h), SD (Ω=30°/h), TD (Ω=45°/h) and QD (Ω=60°/h). The m.s.d. $\sigma(\Omega)$ is used to define a threshold level $t_S\sigma(\Omega)$ where t_S is supposed to be a Student coefficient. Venedikov used the classical value $t_S = 3$ (the 3 sigma rule). VAV04 provides also a tool to relax the Rayleigh criterion for the separation of the nodal waves by numerical experimentation. To decide if a finer separation is justified we can use the Akaike information criterion (AIC, Sakamoto et al., 1986). For a given data set the optimal separation corresponds to a minimal value of AIC. After a systematic experimentation we were able to separate the nodal waves without degrading the AIC value for series close to 3,500 days or 9.5 years as a minimum (Table 4). It is only half of the length based on the Rayleigh criterion.

The separation of the nodal waves is not valid for Bad Homburg and Sutherland as the error on K1 is increased by a factor of two after the separation of $K1^-$ and $K1^+$. We present here the results of 12 GGP stations.

As seen from Table 1, the nodal wave $K1^-$ (1, 1, 0, 0,-1, 0) has a much smaller amplitude than the symmetrical wave $K1^+$ (1, 1, 0, 0, 1, 0) and is thus determined with a much lower precision. The associated RMS errors on the amplitude factors are of the order of respectively 0.15% and 0.02%, corresponding to the inverse of the amplitude ratio. K1 and its nodal companions correspond to the annual modulation of the meteorological wave S1. the tidal factors of $K1^-$ is thus much more affected by environmental conditions. It is clearly seen in the Brussels results, which is not providing a reliable amplitude factor for $K1^-$, although it is the only series longer than 18 years.

A direct comparison of the tidal amplitude factors of $K1^-$, K1 and $K1^+$ given in Table 4 with the theoretical values is not possible as we did not apply any ocean load correction. As a matter of fact we do not have ocean tides models for these nodal waves. We can indeed suppose that, inside the K1 group, the ocean load correction is directly proportional to the amplitudes of the different waves due to the very close frequencies. This hypothesis is not in contradiction with the results of the Oostende tide gauge, given the associated RMS errors (Table 3). We decided thus, as a first approximation of the slope of the resonance, to use the normalized differences

$\rho^- = (\delta_{K1}^- - \delta_{K1})/\delta_{K1} = \delta_{K1}^-/\delta_{K1} - 1$

and (4)

$\rho^+ = (\delta_{K1} - \delta_{K1}^+)/\delta_{K1} = 1 - \delta_{K1}^+/\delta_{K1}$.

It has the advantage to suppress the calibration errors and to reduce drastically the ocean load contribution from the result if the load vector **L** is proportional to the amplitude of the different waves.

Neglecting other perturbation sources than ocean tides we can write

$$\mathbf{A_o} = \mathbf{R} + \mathbf{L} \qquad (5)$$

and derive the two components of $K1^-$ and K1

$\mathbf{A}_\mathbf{o}^-(\delta_{th}^-.A_a^- + L^-\cos\lambda^-, L^- \sin\lambda^-)$ and $\mathbf{A_o}(\delta_{th}.A_a + L\cos\lambda, L\sin\lambda)$

If $A_a^- = x\, A_a$ we state $L^- = xL$, $\lambda^- = \lambda$ to get for K1- and K1

$$A_o^- = \sqrt{(\delta_{th}^- x A_a + xL\cos\lambda)^2 + xL\sin^2\lambda} = \delta_{th}^- x A_a \sqrt{1 + 2L\cos\lambda/\delta_{th}^- A_a + L^2/(\delta_{th}^- A_a)^2}$$

$$A_o = \sqrt{(\delta_{th} A_a + L\cos\lambda)^2 + L\sin^2\lambda} = \delta_{th} A_a \sqrt{1 + 2L\cos\lambda/\delta A_a + L^2/(\delta_{th} A_a)^2}$$

$$\delta^- = A_o^-/xA_a = \delta_{th}^- \sqrt{1 + 2L\cos\lambda/\delta_{th}^- A_a + L^2/(\delta_{th}^- A_a)^2}$$

$$\delta = A_o/A_a = \delta_{th}\sqrt{1 + 2L/\delta_{th} A_a + L^2/\delta_{th}^2 A_a^2}$$

so that we get

$\delta^-/\delta \approx \delta_{th}^-/\delta_{th}$ considering $\delta_{th}^- \cong \delta_{th}$ under the square root

The ocean load contribution is thus largely eliminated from the ratio of the observed amplitude factors, which is then close to the ratio of the body tides amplitude factors.

A similar demonstration is valid for $K1^+$.

5. Discussion of the results

Table 5 presents the relative variations of the amplitude factors inside the K1 triplet using the ρ parameter and the corresponding values for different body tides models. We note that the non hydrostatic models provide lower values of ρ^- and ρ^+ than the hydrostatic ones. It is due to the shift of the resonance toward longer periods. The same results are graphically displayed in Figure 1.

As expected the standard deviation is much larger on ρ^- (0.31%) than on ρ^+ (0.08%). The mean value $\bar{\rho}^- = 0.262\% \pm 0.088\%$ is not really compatible with any of the models. On the contrary the mean value $\bar{\rho}^+ = 1.113\% \pm 0.022\%$ is close to the non hydrostatic models. It confirms the results presented in Ducarme et al., 2009 for the corrected amplitude factor δ_c of

the wave O1 and the ratio $\delta_c(O1)/\delta_c(K1)$, using the data of the West European Network (WEN). The hydrostatic models are offset by a bit more than the associated RMS error.
Looking at Figure 1 there is an obvious correlation (r=0.7) between the observed values of ρ^- and ρ^+. Larger or smaller values of ρ^- are preferentially associated with similar values of ρ^+, the slope of the regression line being close to 3, i.e. the perturbations are three times larger for ρ^- than for ρ^+. It should be noted that correlated extreme values are found also among the WEN stations for which the tidal loading is weak in the diurnal band (Ducarme et al., 2009), while stations with a large loading, such as Matsushiro and Wuhan, do not show any correlation. The perturbations are not due to ocean tides loading but their origin is more likely to be found in the environmental noise concentrated on S1, as K1 corresponds to the annual modulation of S1. The noise propagation around S1 was already pointed out in Ducarme and Melchior, 1998.

6. Conclusions

A strict application of the Rayleigh criterion should limit the separation of the nodal waves to series of 18 years minimum. The longest series of superconducting gravimeters participating to the GGP consortium are now ranging between 10 and 18 years. It was possible to extract successfully the nodal waves for 12 series longer than 3,500 days using the advantages of the VAV04 tidal analysis program. Most of the nodal waves do not provide a new insight into tidal theory with the notable exception of the K1 triplet. The slope of the FCN resonance curve is producing differences in the amplitude factors inside the triplet at the level of 0.1%. This effect is clearly seen in our results. We introduce a parameter $\rho^{\pm} = |1- \delta_{K1}{}^{\pm}/\delta_{K1})|$, free from calibration errors and ocean tides loading influence, to express the relative difference between K1 and its nodal companions $K1^-$ or $K1^+$. The $K1^-$ nodal wave has a too small amplitude to provide reliable results but the mean relative difference ρ^+ between K1 and $K1^+$ (0.113%±0.022%) is very close to the values 0.124% and 0.116% predicted respectively by the DDW99NH (Dehant et al., 1999) and the MAT01NH (Mathews, 2001) models. It should be worth to introduce the nodal wave $K1^+$ in the determination of the FCN parameters, besides O1, P1, K1, PSI1 and PHI1.

Acknowledgements

The data used in this study were extracted from the Global Geodynamics Project (GGP) data base and preprocessed at the International Centre for Earth tides (ICET).

Bibliography

Baker, T. F., Bos, M. S., 2003. Validating Earth and ocean models using tidal gravity measurements. *Geophys J. Int., 152, 468-485*
Crossley, D., Hinderer, J., Casula, G., Francis, O., Hsu, H. T., Imanishi, Y., Jentzsch, G., Kääriaïnen, J., Merriam, J., Meurers, B., Neumeyer, J., Richter, B., Shibuya, K., Sato, T., Van Dam, T., 1999. Network of superconducting gravimeters benefits a number of disciplines. *EOS, 80, 11, 121/125-126.*
Dehant, V., 1987. Tidal parameters for an inelastic Earth. *Physics of the Earth and Planetary Interiors*, 49, 97-116, 1987.
Dehant V., Defraigne P., Wahr J., 1999. Tides for a convective Earth. *J. Geophys. Res., 104,B1, 1035-1058.*
Ducarme B., Melchior P., 1998. Eight lunar nodal waves and third degree waves derived from the 14 year series of observations with the superconducting gravimeter GWR/T3 in Brussels

Proc. 13th Int. Symp. on Earth Tides, Brussels July 22-25, 1997. Observatoire Royal de Belgique, Série Géophysique, Brussels, 347-356
Ducarme B., Sun H.P., 2001. Tidal gravity results from GGP network in connection with tidal loading and Earth response. Proc. 14th Int. Symp. On Earth Tides. *Journal of Geodetic Society of Japan*, 47, 1, 308-315.
Ducarme B., Sun H.P., Xu J.Q., 2002. New investigation of tidal gravity results from GGP network. *Bull .Inf. Marées Terrestres*, 136, 10761-10776
Ducarme B., Sun H. P., Xu J. Q., 2007. Determination of the free core nutation period from tidal gravity observations of the GGP superconducting gravimeter network. *Journal of Geodesy*, 81, 179-187 *(DOI:* 10.1007/s00190-006-0098-9)
Ducarme B., Rosat S., Vandercoilden L., Xu J.Q., Sun H.P., 2009. European tidal gravity observations: Comparison with Earth Tides models and estimation of the Free Core Nutation (FCN) parameters. Proceedings of the 2007 IAG General Assembly, Perugia, Italy, July 2 - 13, 2007, Observing our Changing Earth, M.G. Sideris (ed.), Springer Verlag, *International Association of Geodesy Symposia*, 133, 523-532*(DOI10.1007/978-3-540-85426-5).*
Farrell, W. E., 1972. Deformation of the Earth by surface load. *Rev. Geoph.*, 10,761-779.
Hartmann T., Wenzel H. G., 1995. Catalogue HW95 of the tide generating potential. *Bull. Inf. Marées Terrestres*, 123, 9278-9301.
Hinderer, J., D. Crossley, and R. Warburton, 2007, Superconducting Gravimetry, in: Treatise on Geophysics, Vol 3., eds. T. Herring and G. Schubert, Elsevier
Mathews, P. M., 2001. Love numbers and gravimetric factor for diurnal tides. Proc. 14thInt. Symp. Earth Tides. *J. Geod. Soc. Jpn.*, 47 (1), 231-236.
Melchior P. 1983. The tides of the Planet Earth, Pergamon Press, 641 pp.
Sakamoto Y., Ishiguro M., Kitagawa G. 1986. Akaike information criterion statistics, *D. Reidel Publishing Company, Tokyo*, 290 pp.
Tamura, Y., 1987. A harmonic development of the tide-generating potential, *Bull. d'Inform. Marées Terrestres*, 99, 6813-6855.
Venedikov, A.P., Vieira, R., 2004: Guidebook for the practical use of the computer program VAV – version 2003. Bull. Inf. Marées Terrestres, 139, 11037-11102.
Wenzel, H. G., 1996. The nanogal software: earth tide data preprocessing package. *Bull. Inf. Marées Terrestres, 124, 9425-9439*
Wenzel H.G., 1997a. Tide Generating Potential for the Earth. *Tidal Phenomena, Lecture Notes in Earth Sciences*, Helmut Wilhelm, Walter Zürn and Hans-Georg Wenzel editors, 66, 9-26.
Wenzel H.G., 1997b. Analysis of Earth Tide Observations. *Tidal Phenomena, Lecture Notes in Earth Sciences,* Helmut Wilhelm, Walter Zürn and Hans-Georg Wenzel editors, 66, 59-76

Table 1: Principal nodal waves derived from the potential of degree 2 (W2). Amplitudes are given at 45° latitude

a) diurnal waves

Wave	τ	s	h	p	N'	Angular speed °/hour	Ampl. nm/s^2	δ σ	α° σ°	origin
2Q1-	1	-3	0	2	-1	12.85207978	1.48	1.1554 ±.0077	-0.556 ±.383	nodal
2Q1	1	-3	0	2	0	12.85428619	7.87	1.1518 ±.0015	-0.664 ±.074	Ellipt. Q1
σ1-	1	-3	2	0	-1	12.92493343	1.79	1.1481 ±.0065	-1.320 ±.322	nodal
σ1	1	-3	2	0	0	12.92713984	9.49	1.1480 ±.0012	-0.761 ±.060	variation O1
Q1-	1	-2	0	1	-1	13.39645449	11.22	1.1453 ±.0010	-0.182 ±.050	nodal
Q1	1	-2	0	1	0	13.39866089	59.49	1.1469 ±.0002	-0.212 ±.009	Ellipt.O1
O1-	1	-1	0	0	-1	13.94082919	58.62	1.1490 ±.0002	0.120 ±.001	nodal
O1	1	-1	0	0	0	13.94303560	310.73	1.14935 ±.00004	0.1072 ±.0018	L declin.
LK1-	1	0	0	-1	-1	14.48520390	1.63	1.1518 ±.0078	0.660 ±.386	nodal
LK1	1	0	0	-1	0	14.48741031	8.78	1.1523 ±.0015	0.212 ±.074	Ellipt. O1
(NO1-)	1	0	0	-1	1	14.49448753	0.69	1.1700 ±.0148	1.256 ±.726	nodal
NO1	1	0	0	1	0	14.49669393	24.43	1.1526 ±.0006	0.189 ±.027	Ellipt. $K1^m$
NO1+	1	0	0	1	1	14.49890034	4.90	1.1548 ±.0026	0.354 ±.128	nodal
P1-	1	1	-2	0	-1	14.95672495	1.63	1.1598 ±.0067	0.821 ±.329	nodal.
P1	1	1	-2	0	0	14.95893136	144.55	1.1496 ±.0001	0.228 .004	S declin.
K1-	1	1	0	0	-1	15.03886223	8.65	1.1435 ±.0013	0.394 ±.065	nodal
K1	1	1	0	0	0	15.04106864	436.80	1.13715 ±.00003	0.2813 ±.0013	LS declin.
K1+	1	1	0	0	1	15.04327505	59.28	1.1360 ±.0002	0.310 ±.010	nodal
J1	1	2	0	-1	0	15.58544335	24.44	1.1585 ±.0005	0.151 ±.022	Ellipt. $K1^m$
J1+	1	2	0	-1	1	15.59008516	4.85	1.1544 ±.0023	0.283 ±.112	nodal.
OO1	1	3	0	0	0	16.13910168	13.36	1.1563 ±.0008	0.088 ±.041	3L declin.
OO1+	1	3	0	0	1	16.14130809	8.56	1.1558 ±.0012	0.099 ±.061	nodal
NU1	1	4	0	-1	0	16.68347639	2.56	1.1556 ±.0042	0.377 ±.208	Ellipt. OO1
NU1+	1	4	0	-1	1	16.68568279	1.64	1.1557 ±.0062	0.206 ±.309	nodal

b)semi-diurnal waves

Wave	τ	s	h	p	N'	Angular speed °/hour	Ampl. nm/s^2	δ σ	α° σ°	origin
N2-	2	-1	0	1	-1	28.43752313	2.69	1.1739 ±.0029	3.061 ±.141	nodal
N2	2	-1	0	1	1	28.43972953	71.96	1.1723 ±.0001	3.111 ±.005	Ellipt. M2
M2-	2	0	0	0	-1	28.98189783	14.02	1.1915 ±..0005	2.436 ±.025	nodal.
M2	2	0	0	0	0	28.98410424	375.80	1.18731 ±.00002	2.4446 ±.0009	L princ.
K2	2	2	0	0	0	30.08213728	47.51	1.1939 ±.0002	1.027 ±.007	LS decl.
K2+	2	2	0	0	1	30.08434369	14.16	1.1950 ±.0005	1.178 ±.024	nodal
η2	2	3	0	-1	0	30.62651199	2.66	1.1954 ±.0028	0.359 ±.136	Ellipt. K2m
η2+	2	3	0	0	1	30.62871839	1.16	1.1926 ±.0065	-0.193 ±.310	nodal

Table 2: Principal nodal waves derived from the potential of degree 3 (W_3)
The amplitude is given at 45° latitude

Wave	τ	s	h	p	N'	Angular speed °/hour	Ampl. nm/s^2	δ σ	α° σ°	origin
M1-	1	0	0	0	-1	14.48984571	0.93	1.0866 ±*0123*	1.691 ±*649*	nodal
M1	1	0	0	0	0	14.49205212	6.28	1.0795 ±*0019*	0.922 ±*010*	L Princ.
M1+	1	0	0	0	1	14.49425853	0.81	1.0777 ±*0097*	0.761 ±*517*	nodal
3MK2-	2	-1	0	0	-1	28.43288131	1.10	1.0704 ±.0064	0.410 ±.342	nodal
3MK2	2	-1	0	0	0	28.43508772	6.47	1.0675 ±.0011	0.093 ±.059	L decl.
3MO2	2	1	0	0	0	29.53312076	5.97	1.0658 ±.0012	-0.408 ±.062	L decl.
3MO2+	2	1	0	0	1	29.53532717	1.12	1.0658 ±.0061	-0.065 ±.329	nodal
M3-	3	0	0	0	-1	43.47394995	0.29	1.0383 ±.0137	0.307 ±.758	nodal
M3	3	0	0	0	0	43.47615636	5.23	1.0615 ±.0008	0.461 ±.042	L Princ.

Table 3: Some nodal waves observed by the Oostende tide gage (1945-2006)

wave	Doodson argument	Amplitude (cm)	Amplitude factor
K1-	165.545	0.19±0.06	0.68±0.21
K1	165.555	5.662±0.060	0.409±.006
K1+	165.565	0.64±0.05	0.34±0.03
M2-	255.545	6.03±0.04	16.83±0.10
M2	255.555	181.23±0.04	18.885±0.004
M3-	355.545	0.045±0.025	10.1±5.9
M3	355.555	0.921±.0026	11.69±0.33

Table 4 : K1 and its two nodal waves as observed by the GGP network, **N** number of days
Δ(AIC) : relative diminution of the Akaike Information Criterion after **n** iterations

Station	**N**	**n**	**Δ(AIC)**	**K_1^-**		**K_1**		**K_1^+**	
			%	δ σ	α° σ°	δ σ	α° σ°	δ σ	α° σ°
Brussels	6699	5	-0.16	(1.1338)	0.583	1.13712	0.248	1.1363	0.333
				±.0021	±.108	±.00004	±.002	±.0003	±.016
Cantley	5881	3	-0.16	1.1480	0.612	1.14725	0.586	1.1462	0.648
				±.0015	±.074	±.00003	±.002	±.0002	±.011
Membach	5938	3	-0.45	1.1408	0.337	1.13716	0.280	1.1358	0.308
				±.0011	±.057	±.00002	±.001	±.0002	±.008
Canberra	4450	0	-0,14	1.1299	-0.747	1.12965	-0.831	1.1295	-0.866
				±.0018	±.091	±.00004	±.002	±.0003	±.0013
Metsahovi	4905	3	-0.38	1.1485	0.199	1.13998	0.083	1.1374	0.144
				±.0019	±.093	±.00004	±.002	±.0003	±.0014
Strasbourg	5024	0	-0.29	1.1387	0.379	1.13695	0.269	1.1355	0.276
				±.0014	±.070	±.00003	±.001	±.0002	±.010
Wettzell	4500	0	-1.31	1.1442	0.277	1.13673	0.204	1.1334	0.230
				±.0014	±.072	±.00003	±.002	±.0002	±.011
Medicina	5069	3	-0.94	1.1369	0.859	1.13484	0.355	1.1341	0.405
				±.0014	±.070	±.00003	±.001	±.0002	±.0010
Matsushiro	4008	3	-0.36	1.1928	0.031	1.18466	-0.068	1.1836	-0.127
				±.0021	±.099	±.00005	±.002	±.0003	±.0015
Moxa	3657	3	-0.51	1.1400	0.357	1.13631	0.227	1.1350	0.224
				±.0012	±.058	±.00003	±.001	±.0002	±.009
Vienna	3425	0	-0.72	1.1358	0.216	1.13392	0.204	1.1330	0.246
				±.0021	±.106	±.00005	±.003	±.0003	±.0016
Wuhan	3319	0	-0.60	1.1548	-0.634	1.15350	-0.464	1.1528	-0.570
				±.0032	±.160	±.00006	±.003	±.0005	±.024
theory	Wahr-Dehant-Zschau			1.13326		1.13189		1.13032	
	DDW99 H			1.13330		1.13197		1.13043	
	DDW99 NH			1.13530		1.13405		1.13264	
	Mathews NH			1.13610		1.13494		1.13361	

Table 5: normalised variations of the amplitude factors around K1

Station	**Number of days**	$\rho^- = (\delta_{K1}^- - \delta_{K1})/\delta_{K1}$ %	$\rho^+ = (\delta_{K1} - \delta_{K1}^+)/\delta_{K1}$ %
Brussels*	6699	-0.292	0.072
Cantley	5881	0.065	0.092
Membach*	5938	0.320	0.120
Canberra	4450	0.022	0.013
Metsahovi	4905	0.747	0.226
Strasbourg*	5024	0.154	0.128
Wettzell*	4500	0.657	0.293
Medicina*	5069	0.181	0.065
Matsushiro	4008	0.687	0.089
Moxa*	3657	0.325	0.115
Vienna*	3425	0.166	0.081
Wuhan	3319	0.113	0.061
	mean	**0.262±.088**	**0.113±.022**
	Standard deviation	0.306	0.078
Theory	Wahr-Dehant-Zschau	0.121	0.139
	DDW99 H	0.117	0,136
	DDW99 NH	0.110	0,124
	Mathews NH	0.102	0.116

* stations belonging to the West European Network (Ducarme et al., 2009)

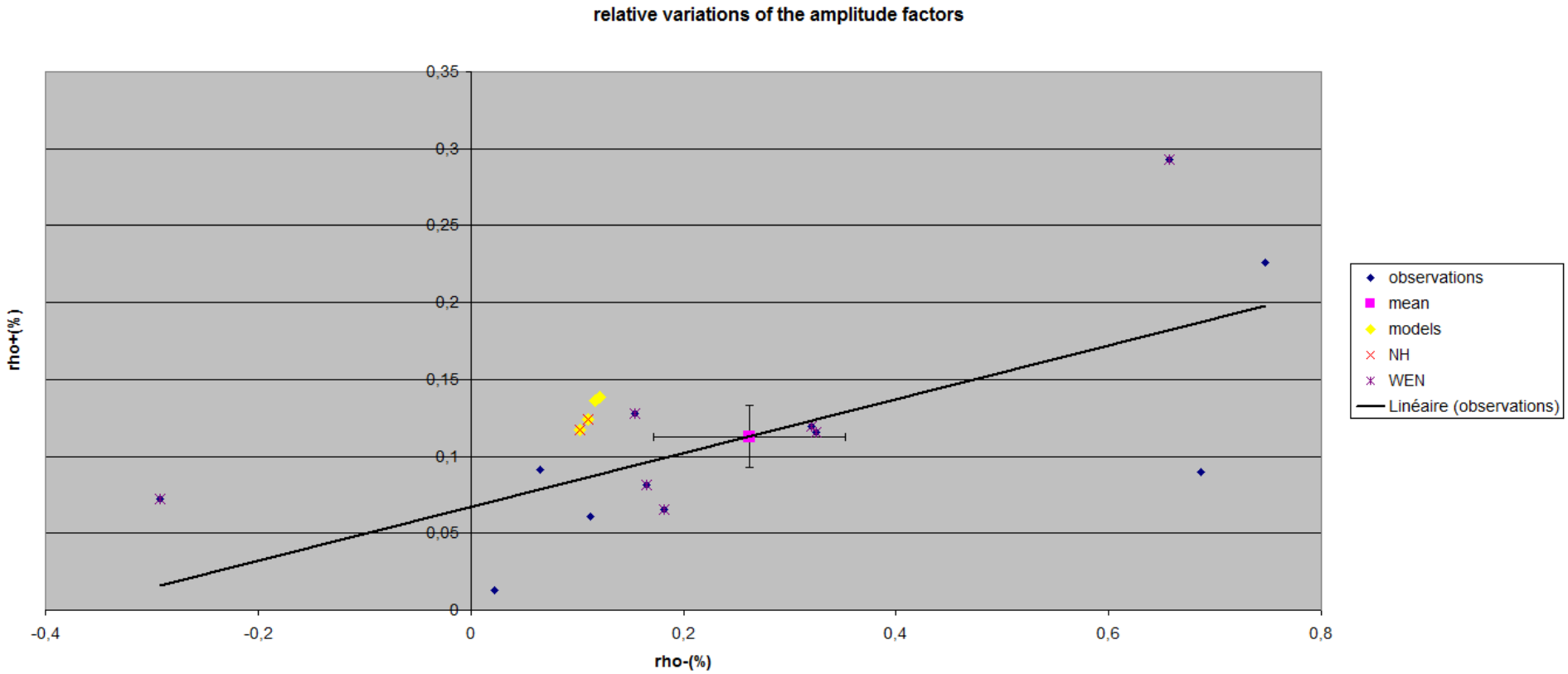

Figure 1: Relative variations of the amplitude factors
$rho^- = (\delta_{K1}^- - \delta_{K1})/\delta_{K1}$, $rho^+ = (\delta_{K1} - \delta_{K1}^+)/\delta_{K1}$
NH: Non Hydrostatic Earth models
WEN: stations belonging to the West European Network (Ducarme et al., 2009)

IAG Commission 3.1 – Earth Rotation and Earth Tides

Business Meeting, IUGG Melbourne, July 1, 2011

Agenda:

1. Welcome, agenda
2. Reports
    a. President
    b. Working groups
        i. Earth Tides in Geodetic Space Techniques (H. Schuh)
        ii. Analysis of Environmental Data for the interpretation of Gravity Measurements (C. Kroner)
        iii. Precise Tidal Prediction (Y. Tamura)
3. Report ICET (J.-P. Barriot)
4. Discussion
5. Election of a new president
6. Other business

Participants:

Gerhard Jentzsch (Germany), Jacques Hinderer (France), David Crossley (USA), Harald Schuh (Austria), Spiros Pagiatakis (Canada), Markku Poutanen (Finland) (until 19.00), Bernd Richter (Germany), Jean-Pierre Barriot (France / Tahiti), Severine Rosat (France), Janos Bogusz (Poland), Yves Rogister (France), Thomas Jahr (Germany), Herbert Wilmes (Germany), Johannes Ihde (Germany) (until 18.50), Peter Schindler (Germany), and about 5 more people.

1. No additions, comments.

2. Reports
    - President's report
        - During ETS 2008, Jena, Earth Tide Medal to two scientists awarded: T. Sato (laudation by W. Zürn), B. Ducarme (laudation by D. Crossley); laudations published in BIM.
        - proceedings of ETS2008 in Special Volume of Journal of Geodesy.
        - more publications in BIM 144 and next two volumes 145 and 146.
        - new location of ICET: University of French Polynesia, Tahiti; J.-P. Barriot as new director.
        - discussion on future of GGP as a service of IAG.
        - renamed Earth Tide Commission medal to **Paul Melchior medal** (family agreed).
        - next symposium will be organized by the National Research Institute for Astronomy and Geophysics (NRIAG), Helwan, Cairo (Egypt), Sept. 24-28, 2012; "The response of the Earth on external and internal forces, including the 17th symposium on Earth Tides"; all subcommissions of commission 3 and inter-commission groups as well as GGP are invited to participate.
        - no questions asked.

i. Report of C. Kroner read by president:
   - at BKG it is discussed to offer a service of 3D reductions of atmospheric influences on SG stations
   - if sufficient hydrologic observations are available, a reduction of these effects for SG stations is possible

ii. Report on Earth Tides in Geodetic Space Techniques (H. Schuh):
   - deformation of the Earth's crust due to atmospheric pressure loading: Vienna model
   - Love and Shida numbers and FCN period from VLBI measurements
   - Tidal variations in earth rotation from VLBI
   - WG should be continued, but maybe another chair more interested in it should be found

iii. Report on Precise Tidal Prediction (Y. Tamura): No report available

3. Report on ICET (J.-P. Barriot)
   - Also available as poster on Sunday 3.
   - New ICET database now available at www.bim-icet.org, www.upf.pf/ICET and maregraph-renater.upf.pf
   - GGP one-minute filtered and manually validated data are routinely processed at ICET and uploaded to ICET and GFZ database; as soon as possible an automated validation shall start. Ideas and Critics on how to improve this tool requested.
   - All BIM issues online at www.bim-icet.org, 25 papers in BIM 144-146 published, 23 related to Jena meeting (server in Paris → broad-band connection.)

4. Discussion
   - ICET directing board will meet again on Monday 4, at noon at the registration desk.

5. Election/Proposal of a new president
   - Gerhard Jentzsch will soon retire and finish his term as president; Spiros Pagiatakis is also not far from retirement and refuses to become new president.
   - Jacques Hinderer refuses.
   - Severine Rosat and Janos Bogusz are asked.
   - G. Jentzsch explains the tasks of president.
   - H Schuh explains problems of decision: president of Comm. 3 has to decide, but Comm. 3 has no new president yet as nominated R. Gross is also nominated for GGOS chair.
   - After discussion Spiros Pagiatakis and Janos Bogusz are nominated as president and vice-president.

6. Other business
   - All other sub-commissions of commission 3 as well as inter-commission study groups as well as GGP are invited to participate the next symposium in Cairo.
   - GGP meeting will be Sat 2.
   - GGP will finish after eight years; new proposal to IAG to continue as a service under IGFS considered.

P. Schindler / G. Jentzsch

International Association of Geodesy

Commission 3, sub-commission 3.1 Earth Tides and Geodynamics

Directoring Board of the International Centre for Earth Tides

Minutes of the meeting held in Melbourne on July 4th, 2011

Note: The name of the subcommission was changed to Earth Tides and Geodynamics

Members of the Directing Board:

Gerhard Jentzsch, past President of the subcommission 3.1
Jean-Pierre Barriot, Director of ICET

Trevor Baker
David Crossley
Olivier Francis
Ruth Neilan
Harald Schuh
Bernard Ducarme
Houtze Xu

1. Present at the meeting were: Barriot, Crossley, Jentzsch, and Schuh.

Baker, Ducarme and Xu as well as Francis were not in Melbourne.

Schuh was again appointed as representative of IAG in the ICET directing board.

All members present agreed, that the Ruth Neilan (rep. of FAGS which does not exist anymore) should be released from her membership, as well as Baker and Hsu because of retirement and no demonstration of interest.

Spiros Pagiatakis as new president of subcomm. 3.1 will become member of the board after reconfirmation by the new president of commission 3.

2. Status of meeting

Those present agreed: Under the above mentioned circumstances this meeting of the Directing Board is a regular meeting.

3. Future of ICET

The future tasks of ICET were discussed as well as the relations to GGP: Barriot explained that funding of ICET was only possible on a yearly basis. He illustrated that he would continue the development of an algorithm for automatic correction of GGP data. A technician was sent to Brussels to study the available software for manual correction. Further, he claimed that the data flow should be standardised. Here, a standard meta data file should be developed.

Barriot reported that he will attend a meeting in September 2011 in Kyoto where the role of ICET as a world data centre would be discussed.

Crossley reported that the groups should correct there 1-minute data of the SG recordings themselves for tidal analyses. IRIS people are interested in the second data. They have created a meta file for seismic stations which should be used as a template for such files for

GGP stations, including calibration history. The long-period data should be corrected either in Strasbourg or at BKG; a one-year test should be started.

Further, the old data should be made available by ICET; here, Ducarme should be involved. Long-term data is a product of GGP.

Concerning BIM, Barriot explained the problems due to different electronic formats. It was agreed that these problems should be solved in the digital way, not by printing the pages and scanning them afterwards, because then all electronic advantages will be lost (like search functions). BIM should be made more attractive by short publication times and at least two volumes per year. Only in this way BIM will regain the old status of a fast information platform for those involved in Earth Tides, ocean tides and geodynamics – in all aspects of theory and experiment.

The website of ICET should be removed from ORB with only a link to the new place, and it should provide links to other related websites.

Schuh pointed out that the terms of reference as well as the size and the names of the members of the directing board should be considered until the next meeting in Cairo.
In any case, the role and missions of ICET should be also re-examined until the Cairo meeting.

4. Other business

No other business

5. Next meeting

The next meeting of the Directing Board will take place during the 17th symposium in Cairo, September 24 to 28, 2012.

July 12, 2011 Gerhard Jentzsch

BLANK PAGE